Geod heights and lithospheric stresses for a dynamic Earth

Article *in* Annales Geophysicae · May 1984

CITATIONS
264

READS
370

3 authors, including:

Yanick Ricard
French National Centre for Scientific Research
190 PUBLICATIONS **7,148** CITATIONS
SEE PROFILE

Luce Fleitout
Ecole Normale Supérieure de Paris
89 PUBLICATIONS **3,253** CITATIONS
SEE PROFILE

Geoid heights and lithospheric stresses for a dynamic Earth

Yanick RICARD, Luce FLEITOUT and Claude FROIDEVAUX

Laboratoire de Géophysique et Géodynamique interne,
Université de Paris-Sud, Bât. 510, 91405 *Orsay, France*

Received 02/08/83, accepted 10/02/84.

ABSTRACT. Mass heterogeneities in the Earth's crust and mantle are known to exist at all depths and for a large range of wavelengths characteristic of their lateral extent. They are the sources of measurable quantities like topography, tectonic stresses and the geoid. Quantitative relationships between these surface observables and deep sources are established for various Earth viscosity structures with spherical symmetry. For an homogeneous mantle, the surface stresses and the geoid height increase with the depth of the perturbing heterogeneity but decrease markedly beyond a critical depth proportional to the wavelength. In the presence of physical or chemical stratification of the mantle, this last decoupling phenomenon is shown to be more complex. The geoid over topography ratio, called the admittance Z, may then change sign. The same is true for the geoid over lithospheric stresses ratio called the Runcorn number Ru. Lower mantle sources are the only candidate capable of explaining the large wavelength geoid undulation with an acceptable magnitude of Z and Ru. This conclusion does not hold if the spherical symmetry of the viscosity structure is broken as it is for the Earth's lithosphere for which the plates are separated by zones of weakness. In this second framework it is shown that upper mantle return flow is also capable of generating the geoid without producing too large a topography and too strong tectonic stresses. The two types of contribution are expected to occur in the Earth. Further progress will require careful data analysis and correlation between topography, stresses, geoid and deep density structures.

Key words : geoid, lithospheric stresses, admittance, mantle heterogeneities.

Annales Geophysicae, 1984, **2**, 3, 267-286.

INTRODUCTION

The surface topography, the prevailing tectonic stress field and the geoid belong to the data set which reflects the internal dynamics of the Earth. Indeed these three observables are known to be linked in some complex way to mass heterogeneities within the deformable Earth. Their value is determined both by the spatial distribution of densities, and by the radial and lateral changes of the mechanical properties at depth. Just by itself, each of the measurable quantities is insufficient to reveal the internal density and viscosity structure. Making use of all of them at the same time ought to be more efficient. The purpose of this paper is therefore to investigate the physical relationships between topography, lithospheric stresses and the geoid. The long term goal is to establish good constraints on the deep dynamical structures.

When the density heterogeneities are of large lateral extent in comparison with their depth, the physical picture is fairly simple. The tectonic style for the lithosphere, i.e. the tendency to thickening or thinning, is determined by a general relationship between the averaged horizontal and vertical stresses, $\bar{\tau}_{xx}$ and $\bar{\tau}_{zz}$ and the moment of the vertical mass distribution within the lithosphere of thickness L (Artyushkov, 1973)

$$\bar{\tau}_{xx} - \bar{\tau}_{zz} = -\frac{g}{L}\int_0^L \rho(z)\, z\, dz \qquad (1)$$

where g is the gravitational acceleration. In this simple form, equation (1) does not include the effects of boundary forces acting either at the edges or underneath the lithospheric plate. The integral representing the moment of the mass distribution in the above equation is also found in the expression of the geoid deviation N caused by the same density distribution (Ockendon and Turcotte, 1977) :

$$N = -\frac{2\pi G}{g}\int_0^L \rho(z)\, z\, dz \qquad (2)$$

where G is the gravitation constant. A good illustration is given by the oceanic plates. Their thermal structure not only explains the topography and the heat flow but also the linear trend of the geoid height (Haxby and Turcotte, 1978; Sandwell and Schubert, 1982), and the age variation of tectonic stresses (Fleitout and Froidevaux, 1983). Equations (1) and (2) show that for shallow sources the ratio of the geoid to average deviatoric stress is independent of the mass distribution. The anomaly defined by equation (2) may be called the

isostatic geoid, in the sense that it assumes perfect compensation within the lithosphere. The knowledge of its amplitude could yield a residual geoid reflecting deeper processes (Hager, 1983*a*). Unfortunately the concept of isostasy lacks a unique definition. Depending upon the choice, the resulting isostatic geoid may differ by up to a factor two (Dahlen, 1982). For example, isostasy defined by cylindrical or conical columns of equal weights is not equivalent to the requirement that the stresses are minimum. This difficulty prompted our attempt to compute the dynamical response to existing mass heterogeneities and thus derive the stresses and geoid height without calling upon the static idea of isostasy.

One should notice however that the geoid undulation caused by lithospheric mass distributions have amplitudes of order 20 m, which have to be compared with overall variations approaching 200 m. Nevertheless a weak global correlation was found to exist between the geoid and the major « tectonic provinces » of the Earth (Souriau and Souriau, 1982). Our approach is not limited to mass heterogeneities within the lithosphere and can well deal with deeper sources in the mantle. It is thus akin to various theoretical attempts to connect models of mantle convection to the observed gravity field (Parsons and Daly, 1983; Lago and Rabinowicz, 1983; Richards and Hager, 1983). For deep sources, the simple equations (1) and (2) do not hold, but interestingly their ratio remains practically unchanged (Runcorn, 1964) as long as the viscosity is uniform. Huge lithospheric stresses due to deep seated mass heterogeneities should therefore be associated with geoid anomalies. But lithospheric stresses seem mainly linked with variations of the structure of the lithosphere (Fleitout and Froidevaux, 1983). This prompted us to search for non-uniform viscosity layering where the geoid anomalies could be associated with moderate lithospheric stresses. Topography seems also mainly related to lateral variations within the lithosphere. This observable helps establishing further constraints upon the mechanical structure of the Earth and upon the origin of mass anomalies which induce the geoid undulations. Dynamically supported topographic variations related to plate motion are equally considered. Their effect on the geoid at large wavelength has to be compared with possible contributions from deep mantle sources.

This paper is divided into four parts. First the appropriate mathematical formulation is derived. In particular it is shown that self-gravitation and compressibility effects have to be included in order to account for long wavelength mechanical responses. Second, the problem is solved analytically for simple spherical Earth structures. This gives a good insight into the geophysical validity of simple expressions like equations (1) and (2) above and also about the relevance of the various concepts of isostasy. Third, the mechanical response to a given density distribution defined in terms of spherical harmonics is computed numerically. This allows to treat a more realistic viscosity and density model of the Earth. The various solutions for surface stresses, topography and gravity are tested with respect to changes in the depth and wavelengths of the assumed density anomaly. This yields a general answer to the question of the validity of simple approximations derived for a flat earth structure, when dealing with the complexity of a spherical self-gravitating stratified planet. In the fourth part, the concepts of admittance and Runcorn number are introduced in order to quantify the relationships between induced geoid and topography, on the one hand, and between geoid and tectonic stresses on the other hand. Furthermore an attempt is made to overcome the limitations caused by the assumed spherical symmetry of the viscosity structures. For this purpose, the dynamic responses of a model Earth with imposed surface velocities are considered.

I. MATHEMATICAL FORMULATION

We consider a model Earth made of a Newtonian fluid with infinite Prandtl number and where both the average density ρ and the viscosity η exhibit a given depth variation. Mass heterogeneities of vanishing thickness are introduced. The induced topography is equally pictured as a surface density. The calculations are carried out in spherical coordinates r, θ, ϕ.

Two cases will be treated. In part II the fluid underneath the lithosphere, which for simplicity, will be called the asthenosphere, is assumed to be inviscid ($\eta = 0$) but compressible. The lithosphere will be described as a compressible fluid in the Boussinesq approximation (Jarvis and McKenzie, 1979). The latter is justified by the fact that the characteristic scale for density variations due to compressibility is of order $K/\rho g$ which amounts to some 5000 km, and thus exceeds strongly the lithospheric thickness. Here K is the bulk modulus.

The continuity and Navier-Stokes equations read :

$$\operatorname{div} v = 0 \tag{3}$$

$$\eta \, \Delta v = \operatorname{grad} p - \rho \operatorname{grad} U + \frac{\rho g}{K} p \tag{4}$$

where v is the velocity vector, U the perturbation gravitational potential and p the excess pressure. The right-hand terms in equation (4) represent the forces due to pressure, self-gravitation and compressibility. To these equations one must add the constitutive law of a Newtonian fluid (Landau and Lifshitz, 1959) which defines the prevailing stresses :

$$[\tau] = 2 \, \eta [\dot{\varepsilon}] - pI \tag{5}$$

where $[\tau]$ represents the stress tensor, $[\dot{\varepsilon}]$ the strain rate tensor and I the identity matrix. Finally, Poisson's equation relates the perturbation gravitational potential to the density :

$$\Delta U = - 4 \pi G \frac{\rho p}{K}. \tag{6}$$

Unlike in part II, compressibility will be neglected in parts III and IV where equations (3) and (5) remain unchanged whereas the right-hand term of equations (4) and (6) is neglected.

The value of g will be kept constant for the whole mantle which is approximatively true for the real Earth. This will not be necessarily consistent with our model density distributions. Only the self-gravitational effect is slightly modified when more realistic density distributions are introduced in numerical models.

In a given spherical shell of density ρ and viscosity η, equations (3) to (6) can be solved in the usual manner (Takeuchi and Hasegawa, 1965; Kaula, 1975; Hager and O'Connell, 1978) by introducing spherical harmonics $Y_l^m(\theta, \phi)$ and the following definitions :

$$
\begin{aligned}
v_r &= u_1(r)\, Y_l^m(\theta,\phi) & \tau_{r\theta} &= u_4(r)\,\frac{\eta_0}{r}\,\frac{\partial Y_l^m}{\partial\theta}(\theta,\phi)\\
v_\theta &= u_2(r)\,\frac{\partial Y_l^m}{\partial\theta}(\theta,\phi) & U &= u_5(r)\,\frac{\eta_0}{\rho_0\, r}\, Y_l^m(\theta,\phi)\\
\tau_{rr} &= u_3(r)\,\frac{\eta_0}{r}\, Y_l^m(\theta,\phi) & \frac{\partial U}{\partial r} &= u_6(r)\,\frac{\eta_0}{\rho_0\, r^2}\, Y_l^m(\theta,\phi)
\end{aligned}
\qquad (7)
$$

where ρ_0 and η_0 are reference values. Let us call V the vector functions $(u_1, u_2, u_3, u_4, u_5, u_6)$ and define a new variable $\nu = \ln(r/R)$ where R is the Earth's radius. By substituting the definitions (7) into equations (3) to (6), one can deduce a system of linear first order differential equations :

$$
\frac{\mathrm{d}V}{\mathrm{d}\nu} = A \cdot V \qquad (8)
$$

where

$$
A = \begin{vmatrix}
-2 & L & 0 & 0 & 0 & 0\\
-1 & 1 & 0 & \dfrac{\eta}{\eta_0} & 0 & 0\\
(12-4\beta)\dfrac{\eta}{\eta_0} & (-6+2\beta)L\dfrac{\eta}{\eta_0} & 1-\beta & L & 0 & -\varepsilon\\
-6\dfrac{\eta}{\eta_0} & 2(2L-1)\dfrac{\eta}{\eta_0} & -1 & -2 & -\varepsilon & 0\\
0 & 0 & 0 & 0 & 1 & 1\\
8\alpha\beta\dfrac{\eta}{\eta_0} & -4\alpha\beta\dfrac{\eta}{\eta_0} & 2\alpha\beta & 0 & L & 0
\end{vmatrix}
$$

In this matrix, there are four parameters $L = l(l+1)$, ε being unity or zero depending on whether the system is self-gravitational or not, $\beta = \rho g R/K$ reflecting the ratio of the Earth radius over the characteristic length of density variations induced by compressibility, and finally $\alpha = 2\pi G\rho R/g$. As can be deduced by inspection of equation (2) the parameter α is a quantity which will appear in the expression of the geoid height as a normalizing factor. For the Earth the last two parameters take the values $\beta = 1.23$ and $\alpha = 0.9$. More generally, for a planet with uniform density, one may write $g = 4\pi G\rho R/3$ and $\alpha = 1.5$.

Within a shell where the various parameters in A are constant, the solution of equation (8) reads simply :

$$
V(\nu) = \exp(A \cdot \nu)\, V(0)\,. \qquad (9)
$$

The exponential in this formula is called the propagator matrix, a quantity which can be expressed analytically (Gantmacher, 1960).

Before solving equation (8) for any specific Earth model, let us go back to the Navier-Stokes formulation given by equation (4). What are the relative magnitudes of the self-gravitation and compressibility terms compared to standard buoyancy ?

To deal with self-gravitation, let us consider a surficial mass $m\, Y_l^m(\theta, \phi)$ at a distance r_m from the Earth center. For an incompressible medium, it defines a potential $U(r, \theta, \phi)$ given by :

$$
U(r,\theta,\phi) = \frac{4\pi G}{2l+1}\, r_m\, \delta m\, Y_l^m(\theta,\phi)\left(\frac{r}{r_m}\right)^n \qquad (10)
$$

with $n = -(l+1)$ upward and $n = l$ downward. The quantity ρ grad U is a body force, the integral of which has to be compared with standard buoyancy, $\delta m\, g Y_l^m(\theta, \phi)$. Averaged radially, the two quantities become $\rho U(r_m)$ and $\delta m\, g Y_l^m(\theta, \phi)$. Their ratio takes a very simple form :

$$
\frac{\langle \rho \,\mathrm{grad}\, U \rangle}{\langle \delta m\, g \rangle} = \frac{\alpha}{l+\frac{1}{2}}\,. \qquad (11)
$$

Self-gravitation becomes therefore a sizable contribution at large wavelengths. For $l = 2$ the above ratio amounts to 45 %. At $l = 9$ which corresponds to a wavelength of 4500 km, it still represents a 10 % correction.

A similar estimation can be carried out for the comparison between the compressibility term in (4) and standard buoyancy. For an inviscid fluid, the excess pres-

sure with angular dependence p is related to the perturbed potential U by the simple equation $p = \rho U$. Thus the relevant body forces related to compressibility become $\rho^2 gU/K$. To the first order, the potential U is always expressed by expression (10). Again an integration is carried out radially to express the average. As U is proportional to r^l the computed averaged body force amounts to $\rho^2 gU(r_m)/(l + 1) K$. The desired ratio is readily found :

$$\frac{\langle \rho g p/K \rangle}{\langle \delta m\, g \rangle} = \frac{\alpha\beta}{(l + \frac{1}{2})(l + 1)}. \qquad (12)$$

Keeping in mind the values of α and β, which are close to unity, one notices that the last ratio decreases more sharply than the previous one. Indeed it predicts a correction related to compressibility of more than 10 % only for the first two harmonics.

II. ANALYTIC SOLUTIONS FOR TWO-LAYER EARTH STRUCTURES

Having established the appropriate mathematical formulation for the mechanical behaviour of a viscous Earth we can now undertake to rephrase the relationship between existing mass anomalies and predicted lithospheric stresses and geoid height. For a simple flat Earth model, these last geodynamical quantities are expected to be proportional to the vertical moment of the density heterogeneities, as predicted by equations (1) and (2). What are the corresponding solutions in the framework of a dynamical, self-gravitational, compressible and spherical Earth ? Do these mechanical solutions vary with wavelength as may be suggested by the l-dependence of the various forces given by equations (11) and (12) ?

Long-wavelength approximation with a viscous lithosphere

The simplest Earth structure to test first is made of a viscous lithosphere of thickness L with mass heterogeneities at its base, and an inviscid asthenosphere extending to its center. At long-wavelengths, ($Ll \ll R$), the mathematical formulation of the problem can be linearised. Thus, at the base of the lithosphere, the variable $v = \ln(r/R)$ becomes $v = -L/R$ and equation (9) yields :

$$V(R - L) - V(R) = -A\frac{L}{R}V(R) + 0\left(\frac{L}{R}\right). \qquad (13)$$

This system of 6 linear algebric equations determines the physical quantities defined in (7). The computation of the solutions requires the definition of boundary conditions at the surface ($r = R$) and at the depth L. The reader who wants to avoid the corresponding algebra is advised to jump directly to the solutions given by equation (20).

For the velocity one has a vanishing vertical component at the surface which implies :

$$u_1(R) = 0. \qquad (14)$$

In the cases treated here, steady-state distribution of density heterogeneities is assumed. In some circumstances, the drift of mass anomalies can induce a time dependent variation of the vertical stress and of the surface velocity. However this surface velocity remains small compared to the velocities inside the mantle.

In the self-gravitational, inviscid asthenosphere the radial stress amounts to $-\rho U$ and its value is discontinuous across the surficial mass heterogeneity $\delta m\, Y_l^m(\theta, \phi)$. This yields :

$$u_3(R - L) = \frac{\delta m\, g}{\eta}(R - L) - \varepsilon u_5(R - L). \qquad (15)$$

One may recall that ε is unity in a self-gravitational system and vanishes otherwise. Shear stresses vanish at the top and bottom of the lithosphere. This requires :

$$u_4(R) = 0 \qquad (16)$$

$$u_4(R - L) = 0. \qquad (17)$$

The last two boundary conditions refer to the potential which at a given depth can be split in two terms deriving from mass distributions above and below

$$U(r) = U^a(r) + U^b(r).$$

Each term has a different radial variation given by equation (10), so that the first derivative reads :

$$\frac{\partial U}{\partial r}(r) = \frac{l}{r}U^a(r) - \frac{l + 1}{r}U^b(r).$$

At the Earth's surface, the topography is a consequence of the computed surface stress $\tau_{rr}(R)$ and is depicted by a surficial mass δm_{topo}, with $\tau_{rr}(R) = \delta m_{topo}\, g$. Following (10) one may thus write :

$$U^a(R) = -\frac{4\pi G}{2l + 1}R\frac{\tau_{rr}(R)}{g}.$$

The last three relations lead to the following boundary condition :

$$u_6(R) = -(l + 1)u_5(R) - 2\alpha u_3(R). \qquad (18)$$

This expression is the same as for an incompressible Earth (Cathles, 1975) because it only involves the mass of the topography.

The situation is not so simple for the last condition at the lithosphere-asthenosphere boundary. Again the potential is split in two parts, and one has :

$$\frac{\partial U}{\partial r}(R - L) = \frac{l}{r}U(R - L) - \frac{(2l + 1)}{r}U^b(R - L).$$

Therefore the potential $U^b(R - L)$ must be formulated. This brings into play both the interface heterogeneity and the asthenospheric density variations caused by compressibility. In the asthenosphere the total potential satisfies equation (6) which takes the form :

$$\Delta U = -4\pi G\frac{\rho^2 U}{K}.$$

This shows that the asthenospheric density variations amount to $\rho^2 U/K$. Through the Earth mantle the seismological data indicates that ρ^2/K varies by a factor smaller than 2. Assuming this ratio to be constant, this last differential equation has the following solutions :

$$U = U(R-L)\sqrt{\frac{R-L}{r}}\,\frac{J_{l+\frac{1}{2}}\left(\sqrt{2\alpha\beta}\,\frac{r}{R-L}\right)}{J_{l+\frac{1}{2}}\left(\sqrt{2\alpha\beta}\right)}\,Y_l^m(\theta,\phi)$$

where J is a Bessel function. The induced density variations contribute to the potential which becomes :

$$U^b(R-L) = -\frac{4\pi G}{2l+1}(R-L)\left[\int_0^{R-L}\frac{\rho^2}{K}\,U(r)\left(\frac{r}{R-L}\right)^{l+2}\mathrm{d}r - \delta m\right]$$

the second term being the contribution of this interface density heterogeneity. The integration yields :

$$U^b(R-L) = \frac{R-L}{R}\,\frac{1}{2l+1}\left(-\,f(l)\,U(R-L) + 4\pi G\,\delta m\right)$$

where the function

$$f(l) = \sqrt{2\alpha\beta}\,\frac{J_{l+\frac{3}{2}}\left(\sqrt{2\alpha\beta}\right)}{J_{l+\frac{1}{2}}\left(\sqrt{2\alpha\beta}\right)}$$

is plotted on figure 1. The sixth boundary condition thus reads :

$$u_6(R-L) = (l+f(l))\,u_5(R-L) - 2\alpha\,\frac{\delta m\, g}{\eta}\,R\,\left(\frac{R-L}{R}\right)^2. \tag{19}$$

We now have six linearized algebraic equations represented by (13) as well as six boundary conditions given by (14) to (19). Exact solutions have been calculated for the six unknown quantities. Three of them have a definite geophysical significance. First, the vertical velocity at the base of the lithosphere which characterizes the lithospheric deformation. Indeed, as the vertical velocity vanishes at the surface, $v_r(R-L)$ determines the averaged radial velocity gradient in the lithosphere, in other words the vertical deformation : thickening or thinning. This quantity $v_r(R-L)$ is of course proportional to the stress $\bar{\tau}_{\theta\theta} - \bar{\tau}_{rr}$. Second, the surface vertical stress $\tau_{rr}(R)$ which expresses the induced topography. Third, the geoid height N which derives directly from the surface value of the potential $U(R)$. The calculated quantities are expressed as follows :

$$\begin{aligned} v_r(R-L) &\approx -\frac{g}{2\eta}\,\delta m\, L\,\frac{l(l+1)}{2l(l+1)-1} \\ \tau_{rr}(R) &\approx \delta m\, g \\ N(R) &\approx -\frac{2\pi G}{g}\,\delta m\, L\,\frac{2l+1+2f(l)-\dfrac{3}{2l(l+1)-1}}{2l+1+f(l)-2\alpha\varepsilon}. \end{aligned} \tag{20}$$

The first expression shows that for a spherical Earth model the lithospheric deformation is still proportional to the dipole moment $\delta m\, L$. In comparison with equation (1), one notices however a weak variation of the proportionality factor with l. This last feature is a consequence of sphericity alone, but not of compressibility or self-gravitation. The second expression exhibits a first term which would correspond to a simple dipole mass distribution, i.e. to a weight of the topography exactly opposite to that of the deep seated mass heterogeneity. However, a complex second term proportional to L and due to dynamical effects which are of course sensitive to self-gravitation and compressibility should be added. The third expression in (20) is equivalent to equation (2) in the limit of large l values. This is depicted in figure 2. Notice that N and δm have opposite signs. An enhancement of the geoid height by 50 % is predicted at large-wavelengths for a self-gravitational Earth model. This departure from equation (2) is roughly in l^{-1}, whereas the weaker correction due to compressibility goes with l^{-2}. In addition to this, the figure shows that sphericity alone produces an effect found about proportional to l^{-3}. These detailed results are in agreement with the estimates of the effects of self-gravitation and compressibility given in the first part of this paper.

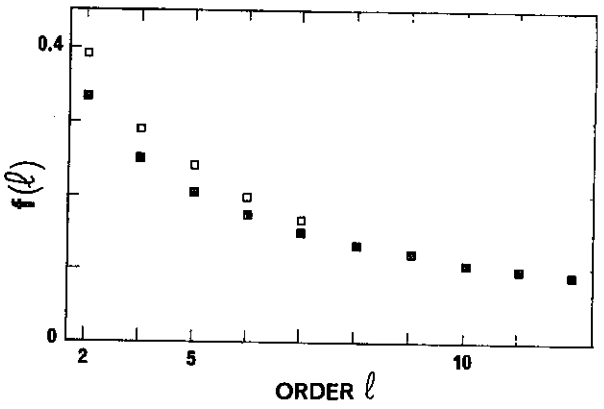

Figure 1

Function $f(l)$ entering into the expression of the geoid height (eq. (20)) for a self-gravitational and compressible model Earth. This Earth has a simple structure consisting of a viscous lithosphere with density heterogeneities at its base and an inviscid asthenosphere. The heterogeneities are represented by a spherical harmonic of order l. The parameter ρ^2/K used to calculate this function can be derived from seismology (Haddon and Bullen, 1969). Here it has been given two different constant values : $6.5.10^{-5}$ S.I. for the black squares and $7.5.10^{-5}$ S.I. for the open squares.

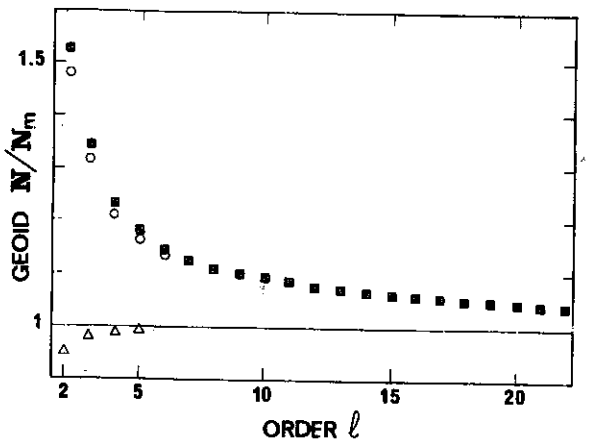

Figure 2

Geoid height normalised to the value predicted by the simple moment law of equation (2) and generated by a shallow-density heterogeneity represented by a spherical harmonic of order l. The model Earth structure is the same as in figure 1. The triangles show the effect of sphericity alone, the circles also include the effects of self-gravitation and finally the squares are obtained by adding compressibility. For this simple two-layer structure which could be treated analytically one sees the marked enhancement of the geoid amplitude at large-wavelengths.

Homogeneous Earth with a thin lithospheric lid

The above model has three limitations in the sense that the asthenosphere is inviscid, the mass heterogeneity is located at the base of the lithosphere, and, that the physical problem has been linearised. These limitations can be avoided and analytical solutions can still be derived if one ignores self-gravitation and compressibility. This approximation has just been found to be valid at moderate-wavelengths ($l > 10$).

The new model Earth structure consists of a spherical homogeneous medium of constant viscosity, containing a harmonic mass heterogeneity at a depth z, and surrounded by a spherical elastic lid of thickness L. The flow induced by the perturbing mass generates stresses at the base of this lithospheric lid. At large enough wavelength ($l < 40$), flexural effects are negligible and the topography amounts to $-\tau_{rr}/\rho g$. On the other hand, the balance of horizontal forces requires that the lateral variations of the averaged tectonic stresses within the lid be determined by the shear forces $\tau^L_{r\theta}$ acting at its base. If one expresses the horizontal lithospheric stress $\tau_{\theta\theta}$ by $\tau_{\theta\theta}(r)\ Y_l^m(\theta, \phi)$, this mechanical condition leads to a vertically averaged value :

$$\bar{\tau}_{\theta\theta} = -\frac{R}{L}\tau^L_{r\theta}. \tag{21}$$

In the absence of self-gravitation ($\varepsilon = 0$) and of compressibility ($\beta = 0$), the propagator matrix A in equation (8) becomes much simpler. The dynamical relationship between velocity and stresses is no longer coupled with the gravitational potential. The vector function $V(r)$ retains only its first four components and A becomes simply a 4×4 matrix. The eigenvalues of the matrix being $l + 1, l - 1, -l, -l - 2$, the solutions in each layer are :

$$\begin{aligned}
u_1 &= ar^{l+1} + br^{l-1} + cr^{-l} + dr^{-l-2} \\
u_2 &= a\frac{l+3}{l(l+1)}r^{l+1} + \frac{b}{l}r^{l-1} - c\frac{l+2}{l(l+1)}r^{-l} - \frac{d}{l+1}r^{-l-2} \\
u_3 &= 2a\frac{l^2-l-3}{l}r^{l+1} + 2b(l-1)r^{l-1} - 2c\frac{l^2+3l-1}{l+1} - 2d(l-2)r^{-l-2} \\
u_4 &= 2a\frac{l+2}{l+1}r^{l+1} + 2b\frac{l-1}{l}r^{l-1} + 2c\frac{l-1}{l}r^{-l} + 2d\frac{l+2}{l+1}r^{-l-2}.
\end{aligned} \tag{22}$$

The coefficients a, b, c, d have to be determined from the boundary conditions. The top layer goes from the lid ($r = R$) to the mass heterogeneity ($r = r_m$), the second layer extending to the Earth's center. The vertical and horizontal velocities u_1 and u_2 must vanish at the contact with the lid. The solutions must remain finite at $r = 0$, so that c and d vanish in the deep layer. At the interface between the two layers, the two velocity components and the shear stress must be continuous and the radial stress jumps by $\delta m\, g$. Thus the solutions are readily established, and in particular the stresses acting under the elastic lid τ^L_{rr} and $\tau^L_{r\theta}$ are now determined. One can therefore express the desired geophysical quantities representing the topography, the tectonic stresses and the geoid. For this one makes use of equation (21) and one computes the effects of both the mass heterogeneity and the induced topography according to equation (10). This leads to the following results :

$$H = -\frac{\delta m}{\rho}\frac{1}{2}\left((l+3)\left(\frac{r_m}{r}\right)^{l+1} - (l+1)\left(\frac{r_m}{r}\right)^{l+3}\right) \tag{23}$$

$$L\bar{\tau}_{\theta\theta} = \delta m\, gR\frac{1}{2}\left(\left(\frac{r_m}{r}\right)^{l+1} - \left(\frac{r_m}{r}\right)^{l+3}\right) \tag{24}$$

$$N = -\alpha\frac{\delta m}{\rho}\frac{1}{2l+1}\left((l+3)\left(\frac{r_m}{r}\right)^{l+1} - (l+1)\left(\frac{r_m}{r}\right)^{l+3} - 2\left(\frac{r_m}{r}\right)^{l+2}\right). \tag{25}$$

One fundamental question addressed here is the following : within what depth range can the geoid height and the lithospheric stresses be expressed by the moment law defined by equations (1) and (2) ? The above solutions were essentially computed to answer this question. The answer is best illustrated by plotting these three quantities as a function of the depth z of the mass heterogeneity and for various values. This is depicted in figure 3. Heterogeneity located at shallow depths induces topography having nearly the same amplitude mass but of opposite sign, as well as tectonic stresses and geoid amplitudes increasing linearly with z. For $\bar{\tau}_{\theta\theta}\, L$, the initial slope is the same as would have been predicted by the simple moment law of equation (1). For the geoid height however, the curves have an initial slope which varies with l. By inspection of equation (25) one sees indeed that this slope is enhanced by a factor $(l + 2)/(l + 1/2)$, with regard to the simple moment law defined by equation (2). Similar result has been obtained from simple equilibrium consideration involving conical columns (Turcotte and McAdoo, 1979; Hager, 1983*a*). For deep seated heterogeneities the various curves depart from these initial linear trends so that the induced topography collapses, and the two other quantities pass over a maximum. This behaviour is characterised by a critical depth z_{max}. The smaller the order l the larger this depth. More precisely $\bar{\tau}_{\theta\theta}$ reaches a maximum value when the source δm is located at a depth z_{max} whereby

$$(R - z_{max})^2 = R^2\frac{l+1}{l+3}$$

therefore one finds approximately

$$z_{max} = \frac{R}{l+3}.$$

For the geoid height the depth of the maximum is somewhat larger, by a factor $(l + 2)/(l + 1)$ and the initial departure from the linear trend is more marked.

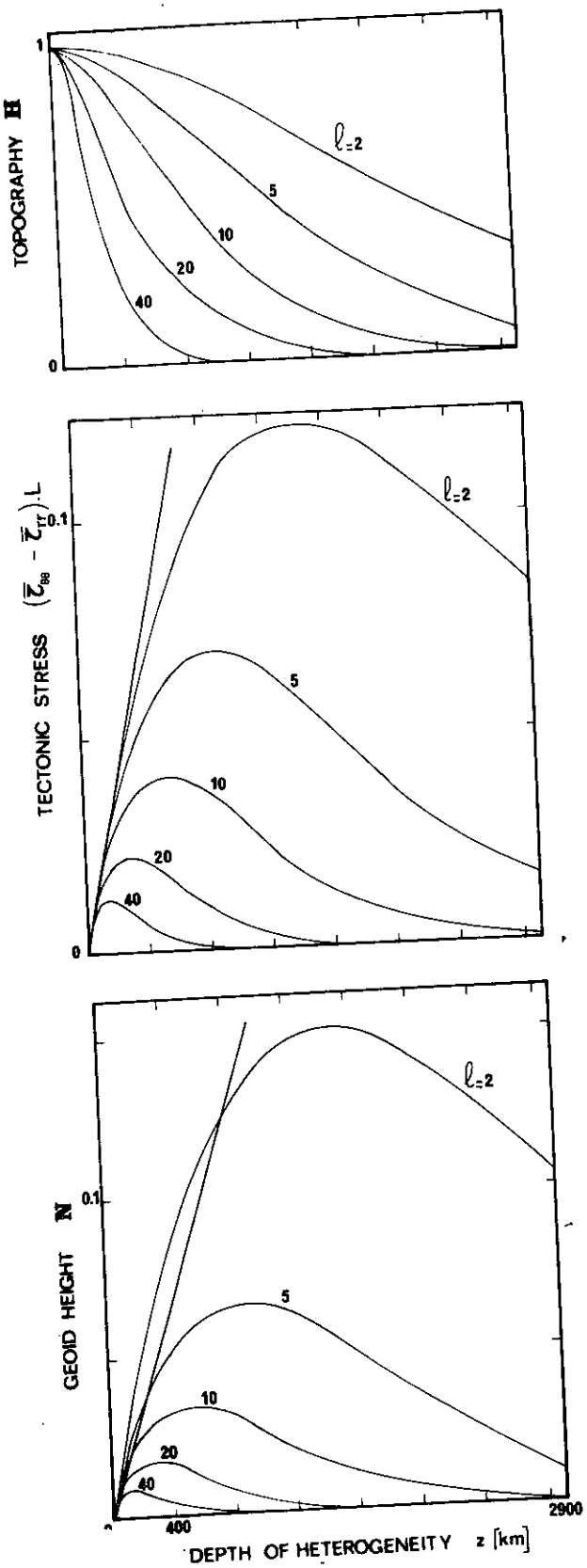

Figure 3

Topography, tectonic stress and geoid height as a function of depth and order of the source density heterogeneity. These solutions were calculated analytically (eq. (23), (24) and (25)) for a non-self-gravitational and non-compressible Earth simply represented by an homogeneous sphere of constant viscosity surrounded by an elastic lid of thickness L. The topography is expressed in terms of $\delta m/\rho$, where δm is the amplitude of the deep mass heterogeneity given per unit surface, and ρ is the topography density. The tectonic stress is the product of the lithospheric averaged deviatoric stress and the lid thickness. It is expressed in units of $\delta m\, gR$. Similarly, the geoid is depicted in units of $\alpha\, \delta m/\rho$ with $\alpha = 2\pi G\rho R/g = 0.9$. One sees that the deeper the source heterogeneity and the shorter its wavelength, the weaker its contribution to surface geophysical observables. The straight lines in the lower graphs correspond to the simple moment laws derived for shallow heterogeneities in a flat Earth as given by equations (1) and (2).

First synthetic remarks

To summarize this chapter, one should emphasize the fact that for simple dynamical Earth models, analytical solutions were obtained in order to predict the geoid height, the topography and the lithospheric deformation caused by density heterogeneities. This is achieved without using the concept of isostasy. In the past, various authors have attempted to express the height of the geoid related to a given mass distribution by starting from the idea of isostasy. The latter has however several non equivalent definitions : cylindrical or conical columns of equal weight (Turcotte and McAdoo, 1979), hydrostatic conditions beyond a certain depth (McNutt, 1980) or minimum averaged deviatoric stresses for the Earth (Dahlen, 1982). All of them imply the existence of a compensation depth L above which any column has an equal weight within possible fluctuations of order L/R. The various definitions of isostasy yield non-identical solutions for the geoid and lithospheric stresses, two quantities related to the moment of the mass distribution. In other words, the formulation of isostasy would have to coincide up to first order in L/R to lead to the same expressions for geoid and stress, these quantities being defined by a first term of order L/R. Here it is worth noticing that the solution derived from an assumed state of minimum deviatoric stress for a self-gravitational Earth (Dahlen, 1982) is the one which is closest to our result shown in figure 2.

Turning to the analytical solutions capable of dealing with deep seated mass heterogeneities one should make some quantitative statements on the magnitude of the quantities shown in figure 3. The geoid height N is given in units of $\alpha \frac{\delta m}{\rho}$. Thus taking a negative density heterogeneity $\delta\rho = -\rho/100$, which could be produced by a temperature excess of some 300 °C, over a thickness of 100 km, one finds that $N = 0.1$ which corresponds to a positive geoid height of 90 m. The same source generates tectonic stresses of magnitude 4 kbar over a 50 km thick lithosphere, and a topography of some 500 m. The general geophysical consequence which can be drawn from these models is that for moderate-wavelengths, say $\lambda < 4000$ km or $l > 10$, the surface observables corresponding to figures 3, 4, and 5, are predominently influenced by mass heterogeneities located within the upper mantle.

It has not been possible to derive simple analytical solutions for a self-gravitational Earth when the mass heterogeneities are deep and of large-wavelengths at the same time. A sizable enhancement of the geoid for low order harmonics has been predicted. For the first model it was caused by self-gravitation. For the second model, which has no self-gravitation, an effect of comparable magnitude occurs because of sphericity alone. The departure from the moment law given by equation (2) must therefore be expected to be sensitive to the chosen radial structure of the Earth's density. This particular problem and other specific geophysical characteristics of the real Earth will now be investigated with the help of numerical methods.

III. THE KEY ROLE OF THE EARTH'S STRATIFICATION

A more realistic model Earth than the simple two-layer structures studied above should include the existence of a core and of transition zones within the mantle. The boundary between two spherical layers can be considered either as purely physical, or as chemical. In the first case the material can flow through the boundary and changes its properties like density and viscosity instantaneously. No undulation of such an interface is considered so that no lateral mass heterogeneity is generated. In the second case, which is well illustrated by the core-mantle boundary, no flow of material is allowed through the interface. The geometry of the latter may however be perturbed, this being equivalent to the creation of lateral mass variations.

The model Earth is made of a succession of spherical shells of thickness l_i, density ρ_i, and viscosity η_i. Compressibility effects, which have just been found to be small, are neglected. In each shell the propagator which appears in equation (9) can be computed in order to determine the solution vector $V(r)$ (Gantmatcher, 1960). The crossing of a mass heterogeneity $\delta m\, Y_l^m(\theta, \phi)$ located at a radial distance r from the Earth's center, demands a jump in the values of two of the six components of the vector function :

$$V = (0, 0, \delta m\, g/\eta\, (r/R), 0, 0, -\alpha\, \delta m\, g/\eta\, (r/R)^2)\,. \quad (27)$$

These two discontinuities were already found in the formulation of the boundary conditions (15) and (19). Free slip conditions are assumed at the Earth's surface and at the core-mantle boundary. The deviatoric stress within the lithosphere is simply proportional to the computed vertical strain rate. At the surface equation (18) still holds. Finally at the core-mantle boundary one induces a surficial mass heterogeneity $\delta m_{cm}\, Y_l^m(\theta, \phi)$ which enters relationships identical to (15) and (19). By eliminating δm_{cm} one finds a single boundary condition

$$u_6 = \frac{R_c}{R}\left(\left(1 + \alpha\varepsilon \frac{\rho_c}{\rho_m}\right) u_5 + \alpha u_3\right) \quad (28)\,,$$

where the subscripts c and m refer to the core and mantle, R_c is thus the core radius. At a physical interface the vector function $V(r)$ is continuous. One ends up with a system of 6 algebraic linear equations where the right-hand side represents the propagation of the discontinuity ΔV of the vector function. One solves numerically for the 6 unknowns, 3 being at the Earth's surface and the other 3 at the core-mantle boundary. First, no other chemical interface will be introduced into the model Earth.

Self-gravitation effect : a numerical test

A three-layer model, called structure (a) made of the lithosphere ($l_1 = 150$ km, $\rho_1/\rho_0 = 1$, $\eta_1/\eta_0 = 1$), an asthenosphere ($l_2 = 2750$ km, $\rho_2/\rho_0 = 1.4$, $\eta_2/\eta_0 = 0.001$), and a core ($l_3 = 3500$ km, $\rho_3/\rho_0 = 3.3$, $\eta_3 = 0$) is first investigated for comparison with the analytical model which ignores the existence of the core and of self-

gravitation. Figure 4 depicts the relevant computed quantities. All solutions are strikingly sensitive to the presence of the core-mantle boundary. When the perturbing mass reaches this interface, it generates a compensating mass of equal magnitude but of reverse sign and the induced velocity and gravity field vanish. Physically this corresponds to the fact that the heterogeneity is floating on the undulating boundary.

Two sets of solutions are shown in the figures in order to appreciate the effects of self-gravitation. The latter is included, ($\varepsilon = 1$) for the full curves, and excluded ($\varepsilon = 0$) for the corresponding dashed curves. As expected, self-gravitation strongly amplifies the geoid at low order l. Here the amplification turns out to be as large as 80 % for $l = 2$. Indeed, the increase of density with depth in the present Earth model favours this effect. Correspondingly the topography is also affected, whereas the deviatoric stresses remain unchanged. Again the straight line drawn on figures can help comparing the solutions with the simple moment laws. For the geoid, the initial slopes are larger in the presence of self-gravitation.

Physical interface at 650 km

A second numerical model, called structure (b), considers the following spherical Earth structure. The viscous lithosphere ($l_1 = 150$ km, $\rho_1/\rho_0 = 1$, $\eta_1/\eta_0 = 1$) surrounds an asthenospheric layer ($l_2 = 500$ km, $\rho_2/\rho_0 = 1$, $\eta_2/\eta_0 = 0.001$). Below 650 km the lower mantle ($l_3 = 2250$ km, $\rho_3/\rho_0 = 1.4$, $\eta_3/\eta_0 = 0.03$) exhibits a marked viscosity increase. The core ($l_4 = 3500$ km, $\rho_4/\rho_0 = 3.3$, $\eta_4 = 0$) is assumed to be inviscid and homogeneous.

The computed geophysical quantities are depicted in figure 5. In comparison with the analytical homogeneous Earth model, this stratified structure yields solutions for the topography with the following characteristics. For mass heterogeneities of long-wavelength, comparable or greater than the Earth's radius R, the new curves differ only slightly from the old ones. For moderate-wavelengths, the sharper drop of the curves shows that mass heterogeneities located within the lower mantle generate very little topography. This means that the more viscous lower mantle sustains this mass more efficiently. The stresses transmitted to the lithosphere become therefore much smaller. Thus figure 5 shows a sharp drop of the rate of lithospheric deformation controlled by $\bar{\tau}_{\theta\theta} L$ as soon as the mass heterogeneity is put close to or into the lower mantle. Finally the solutions for the geoid height exhibit more complexity. For large-wavelengths one notices a reduction of the amplitude but no change of sign. For moderate-wavelengths however, the geoid height changes its sign when the mass heterogeneity is located close to the 650 km boundary. This means that the geoid anomaly is predominently determined by the deep source, rather than by the weak induced topography. As the source is put deeper into the lower mantle, its gravitational attraction at the Earth's surface weakens, whereas the induced topography remains fairly constant. Thus the geoid height changes sign again. This behaviour is only found for l values between 8 and 40. It agrees with the conclusion of other authors having

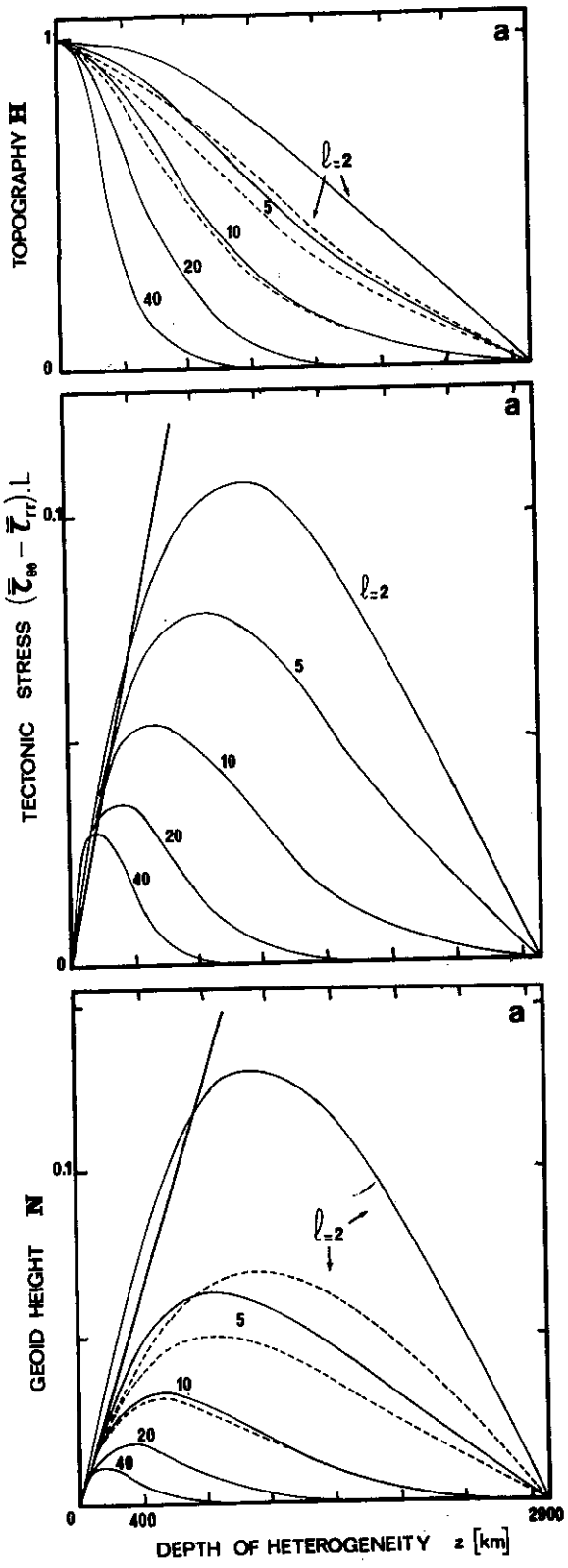

Figure 4

Plot of the same three geophysical observables as in figure (3). *This time the model Earth corresponds to structure (a) : a lithosphere of thickness* 150 km *and of unit density and viscosity, surrounds an asthenosphere of density* 1.4 *and viscosity* 0.001 *extending to an inviscid core of density* 3.3. *Two sets of solutions are given for these uncompressible Earth models : the full curves are with self-gravitation, the dashed curves are without. For tectonic stresses the two curves are undistinguishable. Again one notices that the effect of self-gravitation is sizable for low order l-values.*

studied somewhat simpler Earth structures containing distributed body heterogeneities (Lago and Rabinowicz, 1983; Parsons and Daly, 1983; Hager, 1983*b*, Richards and Hager, 1984).

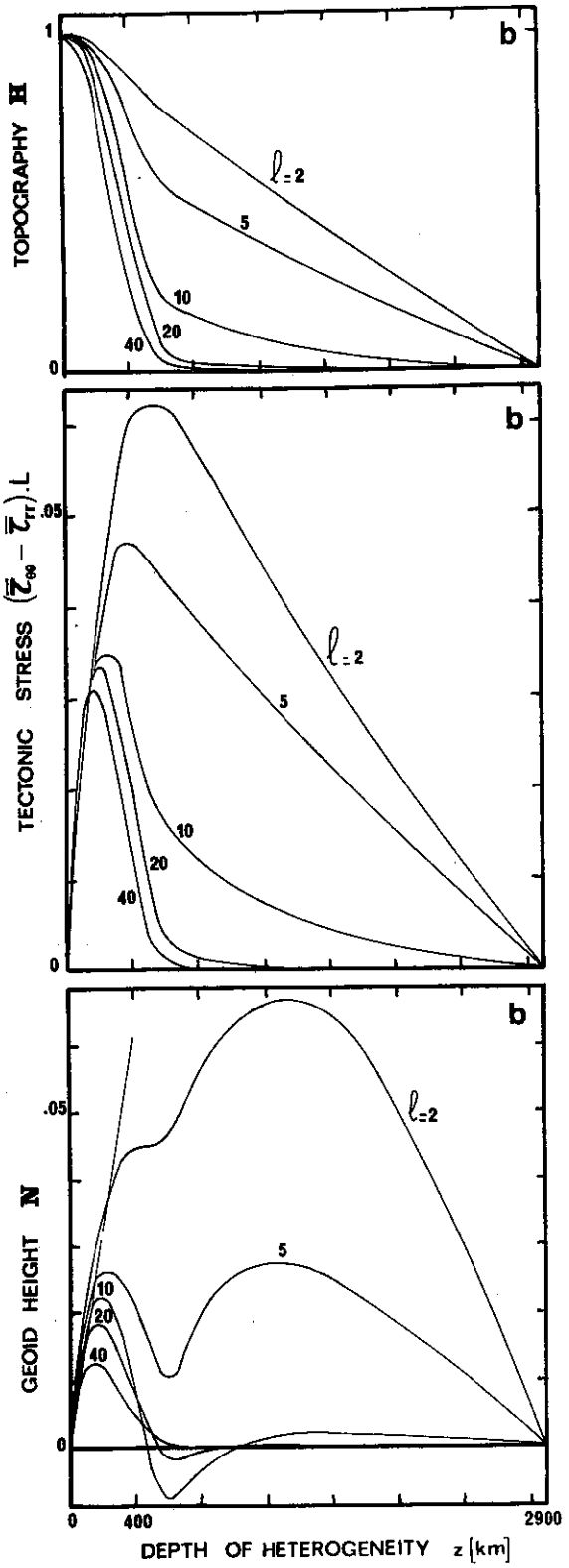

Figure 5

Same plots as in figure 4 but for Earth structure (b), with an added feature, the 650 km upper-lower mantle boundary. The upper mantle has now a unit density and the same viscosity as in structure (a), whereas the lower mantle of density 1.4 has a viscosity 0.03, implying a viscosity contrast of 30 at 650 km. This Earth model is again self-gravitational as are all the following ones. Notice the change of scales with respect to the previous figure for the two lower quantities. For density sources located near or below the new boundary, the computed surface responses have now a smaller magnitude as the stiffer lower mantle is capable of sustaining larger stresses.

Chemical interface at 650 km

The case of a chemical transition between upper and lower mantle will be examined. All other characteristics

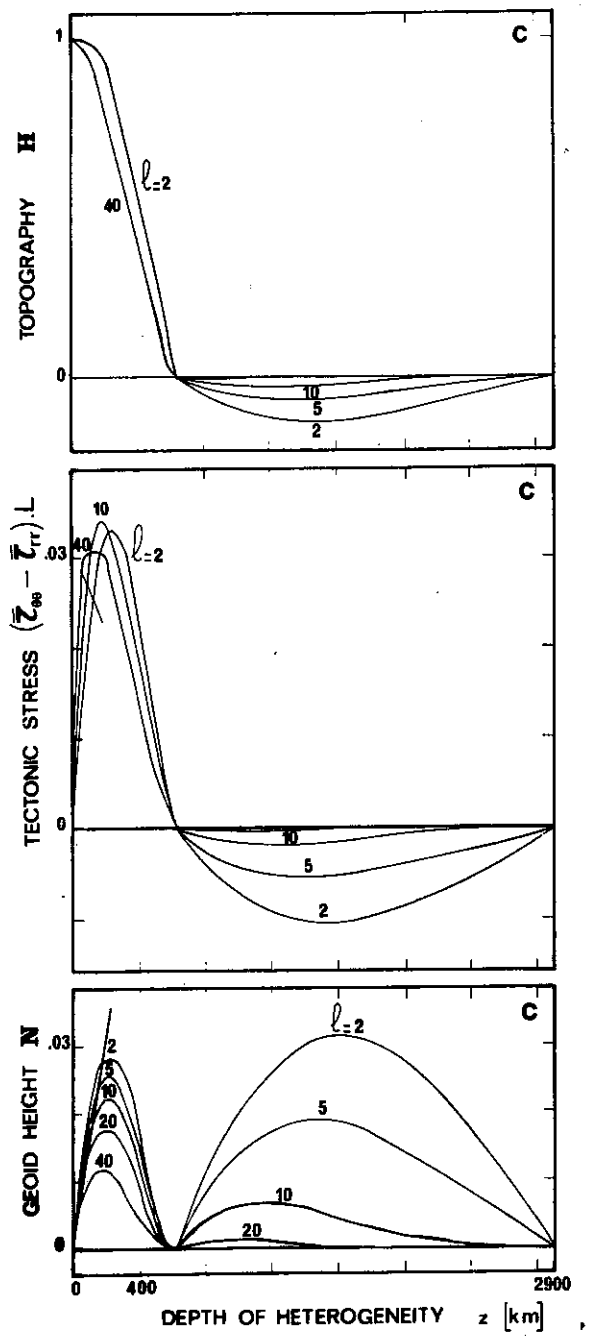

Figure 6

Same plots as in figure 5, for the same model Earth density and viscosity but with the additional requirement that the upper-lower mantle boundary be chemical (Structure (a)). This implies a two-stage flow pattern responsible for the change of sign of the induced topography and tectonic stresses. Notice also that all quantities vanish at a chemical boundary like here at 650 km and at the core-mantle. For pictural simplicity some curves have not been drafted.

of the structure just described remain unchanged. This new Earth model, called structure (*c*), requires a vanishing flow of material through that boundary. In the computation procedure the vertical velocity v_r is made zero by superposing two solutions for $V(r)$. The first one is identical to that already obtained for a purely physical interface. It yields a finite vertical velocity at the 650 km boundary. The second one must induce a compensating flow at this depth and derives from an appropriate density heterogeneity located precisely at this interface. The corresponding geophysical solutions are shown in figures 6.

This new chemical boundary also requires that the three plotted quantities vanish when the mass heterogeneity

reaches this interface. To understand the fact that the topography and lithospheric stresses change sign when the perturbing mass is located in the lower mantle, one should realize that the chemical boundary imposes a two-stage flow pattern. A downwelling current in the lower mantle drives an upwelling flow above 650 km because of the mechanical coupling at the interface. Hence the changes of sign. A positive mass in the upper mantle creates a depression at the Earth's surface which determines the negative sign of the geoid deflection. The same mass located in the lower mantle produces a weak positive surface topography. The strongest contribution to the geoid is however coming from the induced mass deficiency at the 650 km boundary and remains therefore negative. Similar results were obtained by Hager (1983*b*) for a stratified Earth without lithosphere.

Narrow asthenospheric channel

The last two model Earths, (*b*) and (*c*), can still be improved by introducing more structure into the upper mantle. This idea is prompted by the analysis of post glacial rebound and Chandler wobble (Wu and Peltier, 1982; Yuen *et al.*, 1982), combined with considerations about large-scale and small-scale processes governing the dynamics of the lithosphere (Richter and McKenzie, 1978; Fleitout and Yuen, 1983). It has led us to introduce a weaker sub-lithospheric channel and at the same time to reduce the viscosity contrast at 650 km. For this purpose the former asthenosphere is divided into two parts : a 150 km thick sublithospheric channel ($\eta/\eta_0 = 0.0001$) overlying a deeper layer of the upper mantle of thickness 350 km and of larger viscosity ($\eta/\eta_0 = 0.01$).

The computed solutions are drawn in figures 7 and 8. The first figure corresponds to the structure called (*d*) which has a physical interface at 650 km. The second, labelled structure (*e*), has a chemical interface at the same depth. These new solutions do not differ too strongly from those shown in the last two paragraphs. For large-wavelengths the weak sublithospheric channel is not felt by the geoid, although it reduces the tectonic stresses as seen by comparison with structure *b*. For intermediate-wavelengths the shielding effect of the soft channel is seen to operate efficiently. Thus the geoid may now become clearly negative even in the presence of the 650 km boundary.

IV. GENERAL SYNTHESIS AND DISCUSSION

Six spherical Earth structures of increasing complexity have been studied in the last two chapters. No description has been given of the velocity and stress patterns at depth corresponding to the computed solutions. The dynamical response of each Earth model has simply been presented by plotting the induced surface topography H, the averaged deviatoric lithospheric stress $(\bar{\tau}_{\theta\theta} - \bar{\tau}_{rr})$ and the geoid height N. For the real Earth the first and the third of these observables are fairly well measured, especially for spherical harmonics of order l up to 20. Let us notice however, that the Earth's topography is mostly due to crustal thickness variations but not to deeper mass anomalies. It is found useful to describe these quantities by the ratio of their spectral values called the admittance $Z(l) = N(l)/H(l)$. This procedure is similar to the common practice defining an admittance between gravimetry and topography (Lewis and Dorman, 1970). It has the advantage to facilitate the comparison between the available set of data and a given class of model, and has been used successfully to characterize elastic parameters or compensation depth of oceanic plates for simple Airy models (McKenzie and Bowin, 1976, Watts, 1978; Diament, 1983).

Here another meaningful ratio will be introduced : it compares the geoid and lithospheric stresses induced by the dynamics of a given mass heterogeneity. The lack of accurate data on the average tectonic stresses means that the above ratio is poorly known for the Earth. Often, only the sign and azimuth of these stresses is given by in situ measurements (McGarr and Gay, 1978; Zoback and Zoback, 1980; Paquin *et al.*, 1982), seismic focal mechanisms (Sykes and Sbar, 1973; McKenzie, 1978), and geological deformations (Philip, 1980; Mercier, 1981).

This general discussion will also raise the question of the limitation of the dynamical models presented so far, which, unlike the real Earth, do not depart from a purely radial viscosity distribution. To broaden the scope of our investigation, two models with imposed surface velocities, rather than prescribed mass heterogeneities, will briefly be discussed.

Admittance

A shallow mass heterogeneity δm at a depth z, ($z \ll R/l$) compensates a topography $H = -\delta m/\rho g$. The corresponding geoid height expressed by the moment law and already used in equation (20) reads $N_m = -\delta m\, z\, 2\pi G/g$. Thus, in this approximation, the admittance becomes :

$$\frac{N_m}{H} = \alpha \frac{z}{R}. \qquad (29)$$

This simple expression predicts a positive admittance which means that geoid and topographic highs or lows are correlated. It amounts to a value of 1/100 for a compensation depth z located near the moho. Of course, such a compensation structure cannot be invoked for the large-wavelength geoid. Undulations of 100 m would imply topography differences as large as 10 km ! The above argument is restricted to the case of a single source heterogeneity. In the presence of sources of opposite signs at various depths, the resulting admittance can well be negative. A rough analysis of the data for the Earth yields admittance values which are predominantly negative for low orders (Kaula, 1980). It takes the topography without correcting for lateral changes in crustal densities and one might wonder how meaningful this type of analysis is. The data is highly scattered, but values around $-1/10$ are somewhat typical. Another analysis, which is probably more relevant and deals exclusively with

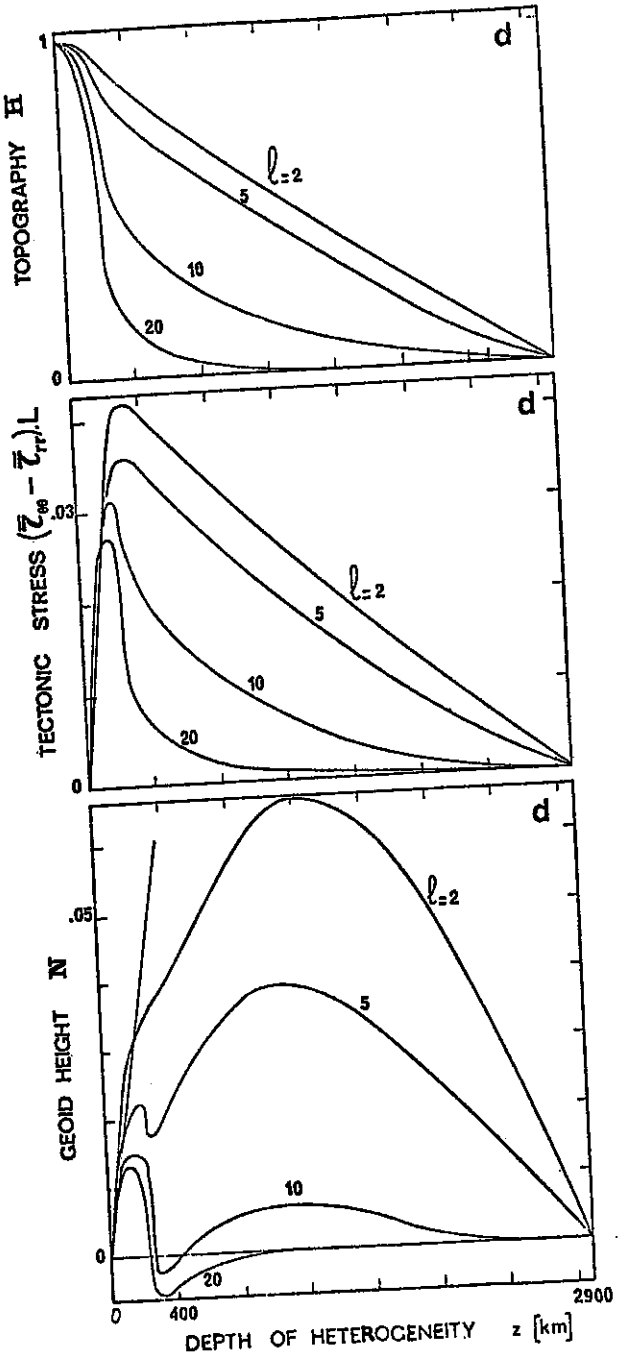

Figure 7
Same plots as in the previous figures but for Earth structure (d) which resembles structure (b) but has an additional sublithospheric channel of very low viscosity. The density structure has not changed, but the viscosity in the upper mantle is now 0.0001 *for the* 150 km *thick channel and* 0.01 *for the remaining layer. By comparison with the solutions for structure (b), one notices the screening effect of the sublithospheric channel.*

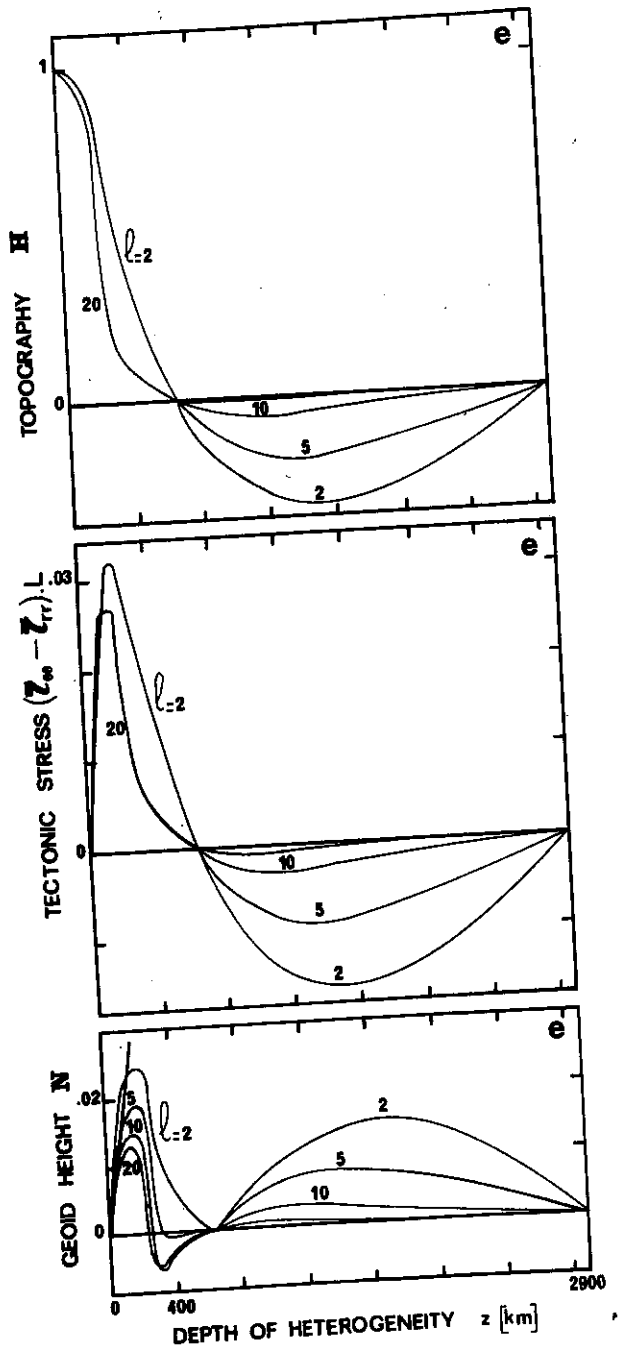

Figure 8
Same plots as in the previous figures for an Earth structure (e) identical to structure (d) but where the 650 km *boundary is now chemical. This feature is seen to produce similar changes as before between figures* 5 *and* 6.

geoid and topography along the axis of oceanic ridges yields, $Z = -0.975$ for $l = 2$ and $Z = 0.332$ for $l = 3$ (Menard and Dorman, 1977). Here a qualitative argument is worth emphasizing. On the one hand, it is well established that the World's ocean floors satisfy a unique topography v.s. age relationship (Parson and Slater, 1977). On the other hand, the large geoid undulations in the oceanic domain do not show any striking correlation with age. This opposition between the two observations can help to define a lower bound for the admittance at large wavelengths. Taking a geoid amplitude of 100 m, and a possible departure to the topography v.s. age relationship no larger than 500 m, one sees that the absolute value of the admittance can be expected to be at least 0.2. Eustatic sea level changes over the past 200 Ma do not seem to differ by more than a few hundred meters from one continent to the other. This also proves that as the continents are drifted over geoid highs and lows, their altitude remains almost constant. This advocates for a high value of the admittance.

Figure 9 depicts the predicted admittance $Z(l)$ for six different Earth structures. In each case 5 depth values of the mass heterogeneity were chosen : the first just below the lithosphere (200 km), the second (400 km)

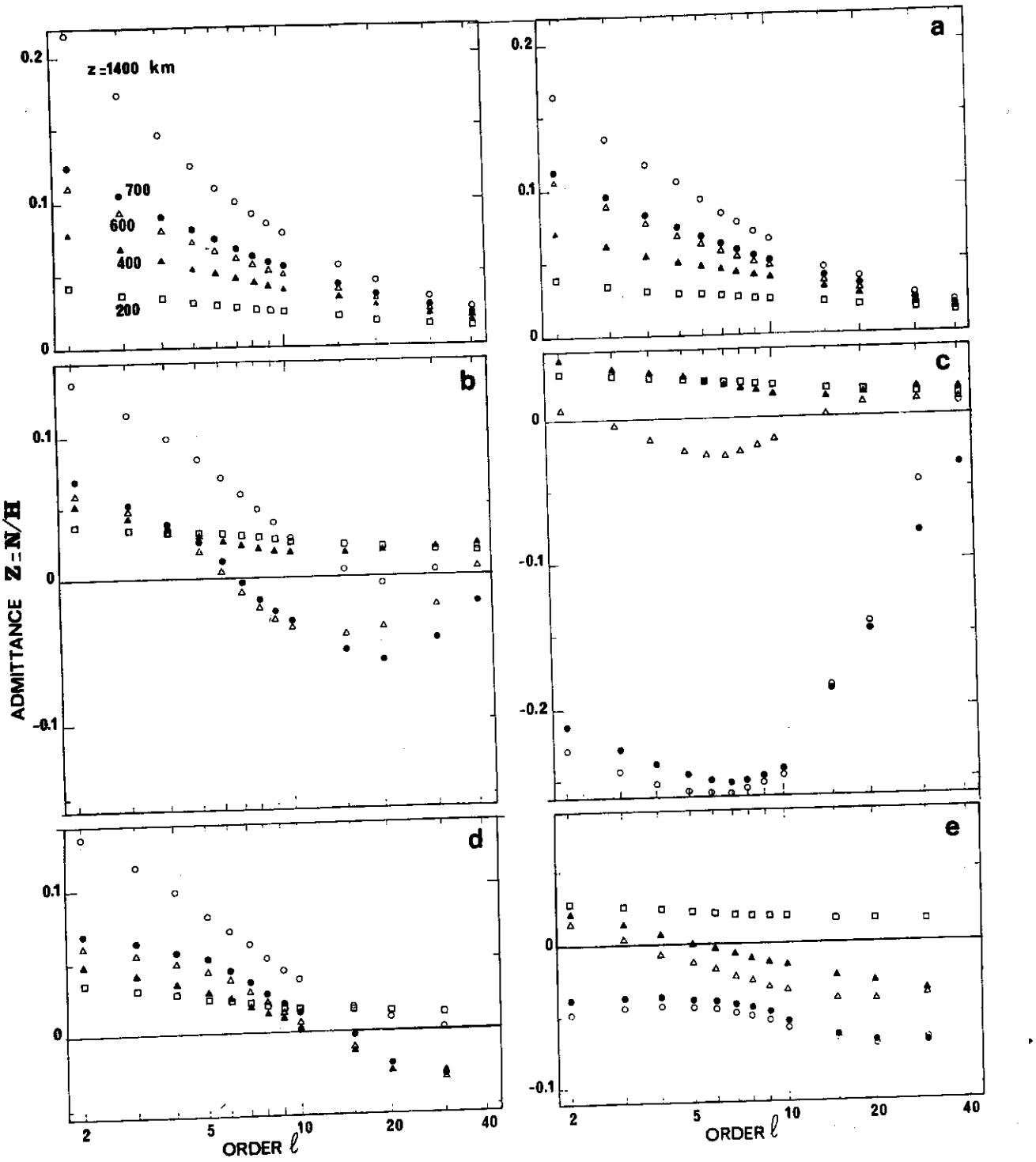

Figure 9

Computed admittances for the analytical model of figure 3 and for the numerical solutions of the model Earth structure (a) to (e). For each case, five different source depths are represented as indicated by different symbols labelled in the top left graph. Beyond $l = 10$ not all points are plotted to avoid overlaps. Notice the existence of negative admittances in particular in presence of a chemical boundary at 650 km *(Structures (c) and (e)).*

and third (600 km) above the interface with the lower mantle, the fourth (700 km) just below this boundary and the fifth at greater depth (1400 km). The curves at the top left correspond to the analytical model Earth with an homogeneous mantle surrounded by a thin lid. Following equations (25) and (23) one has :

$$Z(l) = \alpha \frac{z}{R} \frac{2l + 4 + (l+1) \cdot \frac{z}{R}}{(2l+1)\left(1 + (l+1)\frac{z}{R} - \frac{(l+1)}{2}\left(\frac{z}{R}\right)^2\right)}. \quad (30)$$

For $lz \ll R$ this is equivalent to equation (29) derived from the moment law and a full compensation by the topography. At large l values each curve tends to vanish showing that the departure from simple l-independent relationships is even more drastic for the geoid than for topography. When the mantle is assumed to be homogeneous, one notices that the admittance is always positive. This was found to remain true with a mantle viscosity decreasing with depth and with the inclusion of a core. An illustration is given at the top right of the figure corresponding to the self-gravitational Earth model of figure 4.

A marked viscosity increase at depth leads to a reversal of sign of the admittance. As shown in the middle and lower rows of the figure 9, a chemical interface between upper and lower mantle (right-hand side curves) favors this trend. The presence of a narrow asthenospheric channel (bottom row) is not well perceived by the admittance. These results demonstrate that, if the real Earth, like the present models had a viscosity structure with spherical symmetry, the observed long-wavelength geoid and topography could not be derived from upper mantle sources. Indeed, shallow sources yield admittance values smaller than 0.1. Lower mantle heterogeneities turn out to be the better candidate, the most favourable case apparently being that of structure *c* which implies a chemical interface at the lower-upper mantle boundary. This opinion is strengthened by looking at the predicted stresses.

Runcorn number

In order to compare the geoid height N to the averaged force deforming the lithosphere $(\bar{\tau}_{\theta\theta} - \bar{\tau}_{rr})\, L$, one may first consider the simple relationships (1) and (2) derived for shallow sources in a flat Earth. Both quantities being proportional to the moment of the mass distribution, their ratio is a constant :

$$\frac{N}{(\bar{\tau}_{\theta\theta} - \bar{\tau}_{rr})\, L} = \frac{2\,\pi G}{g^2}. \qquad (31)$$

It amounts to $4.4.10^{-7}$ bar^{-1}. This ratio is positive, indicating that geoid highs are correlated with regions of more extensional tectonics. The ridge push and the geoid maximum associated with ridges provide a quantitative illustration of this relationship. For a lithospheric thickness $L = 50$ km, it implies 550 bar stresses for 12 m of geoid (Fleitout and Froidevaux, 1983).

Longer wavelength geoid undulations have amplitudes one order of magnitude larger than that. Are they associated with proportional stress variations which follow from equation (31) ? If so, these would dominate the global lithospheric stress pattern. Observations preclude such a conclusion. Indeed, stresses often change sign over short distances between neighbouring tectonic provinces showing that short-wavelength shallow sources often dominate the stress field. Numerically one may say that the stress variations associated with the large-wavelength geoid of amplitude 100 m are unlikely to exceed 1 kbar.

These last remarks suggest that equation (31) does not apply for all wavelengths and all depths of the sources. This can readily be demonstrated on the basis of analytical solutions. The first study relating geoid height and surface stresses for an homogeneous Earth was performed by Runcorn (1964). Our solutions are slightly different as we assumed no variations of g with depth. We shall call Runcorn number the normalised ratio :

$$Ru = \frac{N}{(\bar{\tau}_{\theta\theta} - \bar{\tau}_{rr})\, L}\,\frac{g^2}{2\,\pi G}.$$

Following equations (25) and (24), for an homogeneous Earth with a thin lithospheric lid, one finds :

$$Ru = \frac{2\,l + 4 + (l+1)\,\dfrac{z}{R}}{(2\,l+1)\left(1 - \dfrac{z}{2\,R}\right)}. \qquad (32)$$

This weak dependence is illustrated in the top left corner of figure 10, which depicts the Runcorn number for our 6 different Earth structures. It shows that for the same geoid amplitude, the deepest long-wavelength heterogeneity generates lithospheric stresses which are two times weaker than those generated by long-wavelength shallow sources.

In the presence of a viscosity increase for the lower mantle the computed Runcorn number displays a more striking pattern (middle and bottom rows). At first glance the sets of curves are very similar to those describing the admittance. The change of sign indicates that a geoid high can now correlate with maximum compression. Like the admittance, these last results point to the fact that a chemical transition and a viscosity contrast within the mantle favour the generation of a sizable geoid anomaly with moderate-surface stresses by deep seated density sources. The absolute value of *Ru* is found to be at most 6 as shown for structure *c* and *d*. Going back to the numerical estimate made above, one expected *Ru* to exceed the value of 4.

The analysis carried out so far, points to deep heterogeneities to explain the large-wavelength geoid. Nevertheless correlations exist between the large-wavelength shape of the geoid and the distribution of subduction zones, indicating the possibility of upper mantle sources. The same is true with the hot spots (Crough and Jurdy, 1980). This problematic conclusion has prompted us to examine models of a different type.

Models with imposed surface velocity

Assuming that seismology were capable of describing the exact distribution of mass heterogeneities within the Earth, can one expect the dynamical models treated above to predict the observed plate tectonic velocities ? The answer is negative for the simple reason that the spherical symmetry of the viscosity structure denies the very existence of plates. Put in another way this argument means that for a purely radial distribution of viscosities, mass heterogeneities can only induce a spheroidal flow. The plate velocity pattern for the Earth shows that the toroidal component is as important as the spheroidal one (Hager and O'Connell, 1978). Hence the hint that the models presented so far are only capable of accounting for part of the real geoid.

Another approach becomes imperative, already suggested by Hager and O'Connell (1978, 1979). It consists in splitting the Earth into a central part which keeps the spherical symmetry and an outer shell, the lithosphere, with a viscosity structure which varies laterally. Zones of mechanical weakness, the plate boundaries, allow moderate driving forces to maintain sizable plate velocities without contributing too much to the geoid. For instance the already mentioned ridge push is

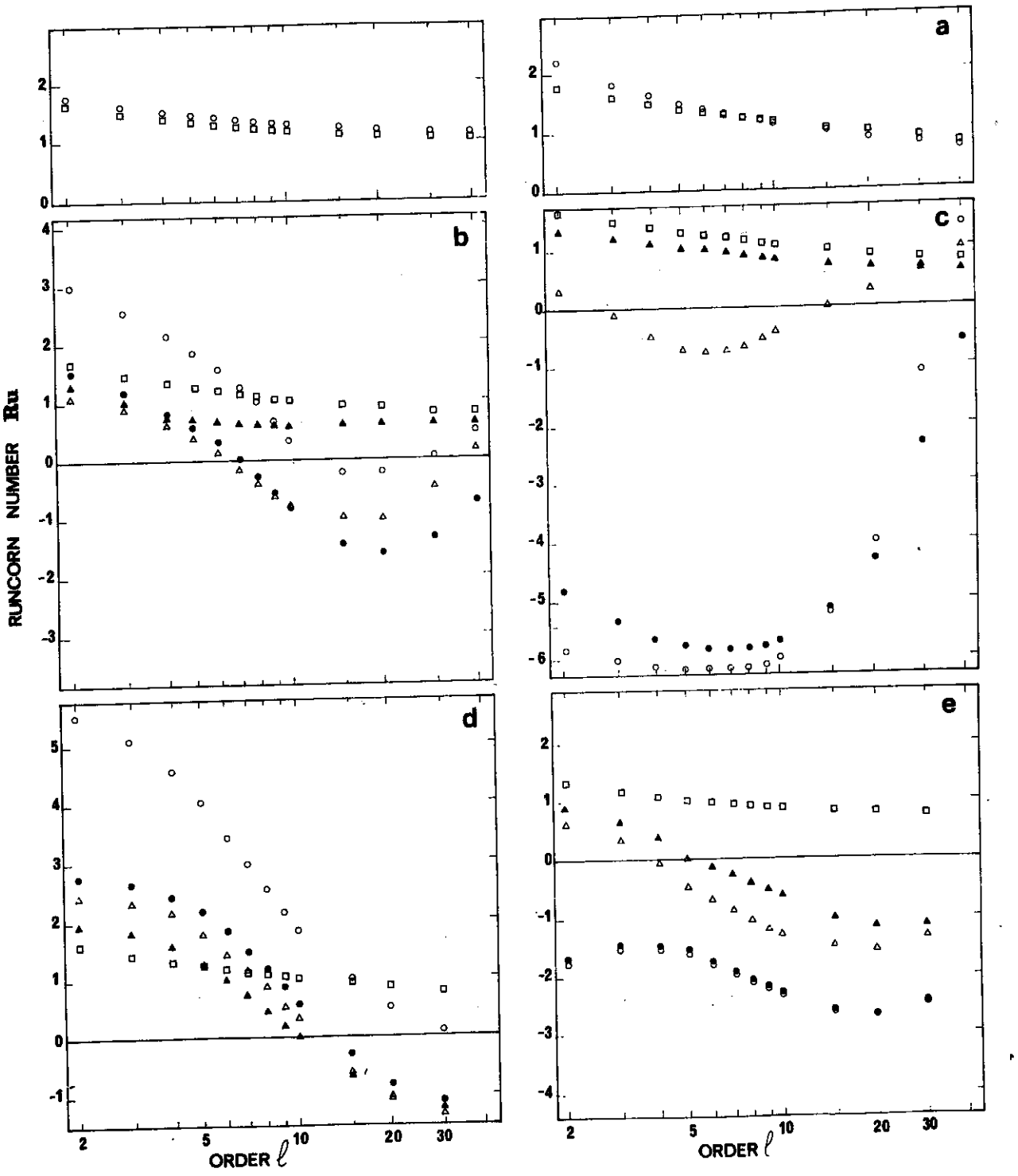

Figure 10

Computed Runcorn numbers of the same 6 model Earth structures for which the admittance was given in the previous figure. All symbols retain the same meaning. One notices that structure (d) characterized by the presence of a sub-lithospheric low viscosity channel leads to the largest Ru values, i.e. minimizes the induced tectonic stresses for a given induced geoid amplitude. In the top two graphs the results for intermediate depths fall between the two sets of points.

known to produce only some 10 to 20 m of geoid deflection. The problem is therefore to investigate the effect of the plate velocities on the central sphere. The necessary return flow is driven by a pressure gradient which also generates topography (Schubert *et al.*, 1978; Hager and O'Connell, 1979) and of course geoid.

Let this sublithospheric Earth consist of an asthenospheric channel of thickness d surrounding a rigid lower mantle. This makes a simple analytical calculation possible. It starts from equations (22). The boundary conditions are defined by having zero vertical and horizontal velocity at the base of the channel of thickness d and viscosity η. At the top, the vertical velocity also vanishes, whereas the horizontal component v_0 is prescribed. In this situation one should realize that the maxima and minima of the surface velocity field are out of phase with those of the topography, geoid and averaged tectonic stress. Therefore the plate surface velocities must in principle be decomposed in terms of $\frac{\partial}{\partial\theta} Y_l^m(\theta, \phi)$. These functions are not normalized and the coefficients v_0 amount approximately to the plate velocity divided by l. This remark is useful if numerical estimates are carried out.

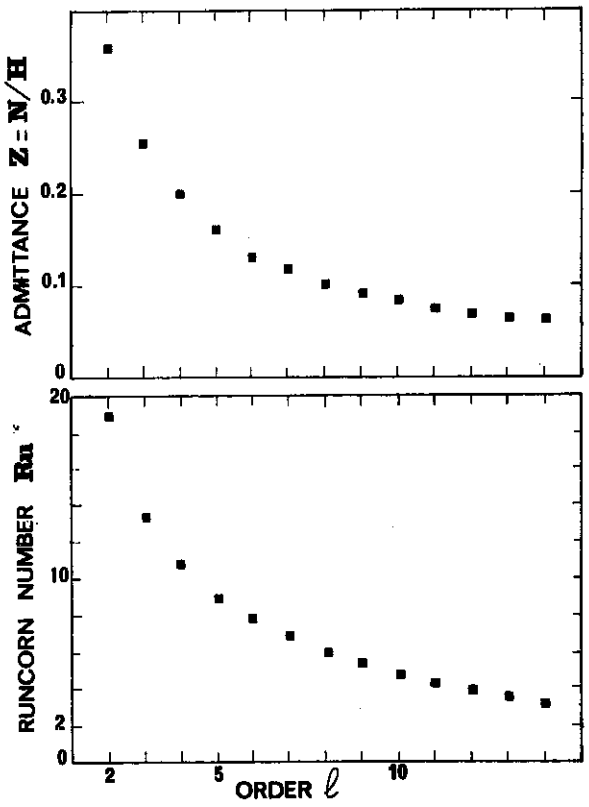

Figure 11

Computed admittances and Runcorn number corresponding to the topography, tectonic stress and geoid induced by an imposed surface velocity expressed in terms of $\partial Y_1^m/\partial\theta$. These results are based on equations (35) *and* (36) *giving approximations of the analytical solutions obtained for a narrow return flow channel with thickness* 200 km. *The two parameters can take up a large positive value.*

After a somewhat cumbersome algebra one finds involved expressions for the stresses $\tau_{r\theta}^L$ and τ_{rr}^L acting at the base of the lithosphere. As before, these quantities directly express the topography and the induced averaged lithospheric stress. For $d \ll R/l$ they become :

$$H = \frac{6\,\eta v_0\,R}{\rho g d^2} \tag{33}$$

$$\bar{\tau}_{\theta\theta}\,L = \frac{4\,\eta v_0\,R}{d}.$$

The absence of an explicit l-dependence must be corrected by the implicit l-dependence attached to the definition of v_0. Thus, H and $\bar{\tau}_{\theta\theta}\,L$ are about inversely proportional to l for a given velocity amplitude.

Another approximation can be derived as d approaches R, i.e. for an homogeneous Earth :

$$N = 3(l+1)\frac{\eta v_0}{\rho g R} \tag{34}$$

$$\bar{\tau}_{\theta\theta}\,L = (2l+1)\,\eta v_0\,.$$

These results indicate that both quantities are proportional to the plate velocity and to the asthenospheric viscosity. Furthermore a narrower channel requires larger stresses, the topography being inversely proportional to d^2 and the tectonic stress to d. Indeed the imposed surface velocity requires a channel return flow which is driven by a horizontal pressure gradient giving rise to the induced topography. The latter is the only mass heterogeneity present in the system. Thus, gravity is simply determined by this monopole. In this situation the admittance takes the simple form :

$$Z = \frac{\alpha}{l+\frac{1}{2}}. \tag{35}$$

Similarly, the Runcorn number does not contain the velocity. On the other hand for small d values it exhibits a proportionality to d^{-1}, as seen in combining equations (33) and (35) :

$$Ru = \frac{3}{2l+1}\,\frac{R}{d}. \tag{36}$$

As d approaches R the combination of (34) and (35) yields :

$$Ru = \frac{3}{2}\,\frac{l+1}{(l+\frac{1}{2})^2}. \tag{37}$$

These results are plotted in figure 11. Obviously, large Ru values are easily obtained for thin return flow channels. At the same time the dynamically supported uncompensated topography yields large Z values at large-wavelengths.

The present exercise aimed at taking the hard facts of plate tectonics in consideration. It hints at two fundamental conclusions. One is that upper mantle processes are capable of generating sizable geoid anomalies without creating too large a topography and too strong tectonic stresses. The other is that lateral variations of the viscosity and of the thickness of the asthenospheric channel would lead to corresponding strong changes in the values of the geophysical observables.

From (33), (35) and (36), one may derive numerical estimates. Taking a surface plate velocity of 5 cm/year, a channel viscosity of 10^{20} poise over a depth range of 200 km, a plate thickness of 50 km, one can compute all the relevant geophysical quantities for order $l = 4$. Equations (33) to (37) yield the following values :

$$H = 510\text{ m} \quad \bar{\tau}_{\theta\theta}\,L = 405\text{ bar} \quad N = 103\text{ m}$$

$$Z = 0.2 \quad Ru = 10.5\,.$$

These quantities are all fairly large. Of course, this simple structure, where all the return flow is confined to a narrow channel, constitutes an extreme case.

More complex deep structures were investigated numerically. The results again show the effect of a viscosity contrast at 650 km, of a chemical boundary at the same depth and of a low viscosity channel below the lithosphere. The numerical procedure starts with the same propagator equation as before but, of course, no imposed mass heterogeneity is present and the free slip boundary condition at the surface is replaced by the imposed surface velocity. In the case of a chemical boundary at 650 km, the vertical velocity at this depth has to be made zero. As before, this is achieved by

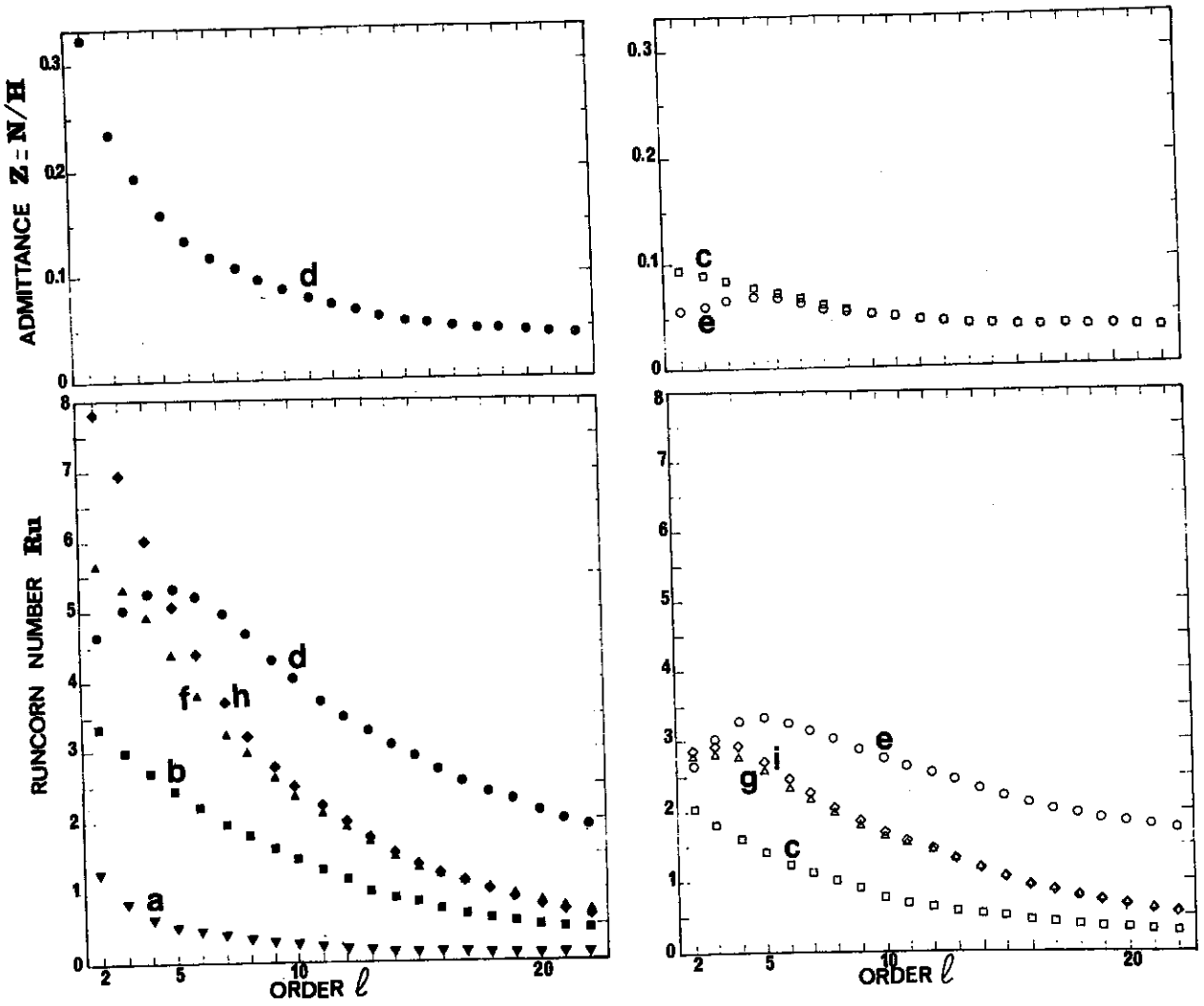

Figure 12

Admittances and Runcorn numbers computed for 9 different Earth structures corresponding to the topography, tectonic stresses, and geoid induced by imposed surface velocity. Structures (a) to (e) are identical to those introduced in chapter III, except for the fact that the rather stiff lithosphere is left out. The next four structures derive from (d) or (e), but a weak 100 km *thick lithosphere has been introduced in order to reinforce the mass return flow. In structures (h) and (i), this return flow is somewhat more confined to the asthenospheric channel as the viscosity underneath it has been multiplied by a factor* 2. *Notice that the solutions on the right-hand side correspond to structures where the* 650 km *boundary is chemical. The corresponding structures with a physical boundary at* 650 km *are found on the left-hand side. Thus (b) and (c), (d) and (e), (f) and (g), (h) and (i) differ only by the nature of the upper lower-mantle interface.*

superposing two solutions. The first is driven by surface velocity, whereas the second is identical to that already used in chapter III and is driven by a mass heterogeneity at the 650 km interface.

Figure 12 depicts the admittances (top) and the Runcorn numbers (bottom) for 9 different structures. The first 5 are identical to structures (*a*), (*b*), (*c*), (*d*) and (*e*) defined in chapter III but for the fact that the outer layer, the lithosphere is now absent. The last two of these structures have a narrow asthenospheric channel of 150 km.

Its thickness is now chosen equal to 200 km. The further four structures retain the asthenospheric channel. The latter is however overlain by a lithospheric layer which has been introduced in order to increase the mass flow. Thus structures (*f*) and (*g*) are obtained by adding a 100 km thick lithosphere to structures (*d*) and (*e*). This lithosphere is only 10 times more viscous than the material below to make its deformation possible. Finally, for structures (*h*) and (*i*), the viscosity of the two layers beneath the asthenospheric channel is enhanced by a factor 2.

The numerical solutions confirm the prediction of the simple analytical model, that the Runcorn numbers are inversely proportional to the channel width *d* as seen by comparing (*b*) with (*d*), or (*c*) with (*e*). This breaks down at large-wavelengths because the return flow can no longer be restricted to the channel. Another striking feature is the divergence of the pairs of curves with and without chemical interface at low order *l*. The curves, for structures with a chemical boundary within the mantle (right-hand side of figure 12), always lie below the corresponding curves where this boundary is only physical (left-hand side). This is caused by two effects. First the geoid is reduced by the presence of a mass induced at 650 km. Second, the confinement of the return flow in the upper mantle somewhat enhances the stresses. When the 650 km boundary is physical, the admittances are very close to equation (35), the small difference coming from the mass induced at the core-mantle interface. In the case of a chemical boundary at 650 km, the admittances are reduced and take a value very close to that of a simple dipole. They do not strongly depend upon the viscosity structure.

Table 1 contains numerical values of the computed geophysical observables for $l = 4$, and an imposed velocity parameter $v_0 = 5$ cm/yr. The 9 structures are listed in the first column. Each structure derives from the previous one in the list and the new added feature is given as a reminder.

One sees that surface velocities imposed by the plates are likely to induce a sizable contribution to the observed geoid. However somewhat larger viscosities would be necessary to obtain 100 m of geoid undulation. Various models of surface deflection due to the present plate motion have been calculated previously (Hager and O'Connell, 1979). The correlation with the observed gravity field is not perfect but these simple models cannot take account of lateral variations of the viscosity and thickness of the asthenospheric channel, like may be the case in the Earth between cratons and oceans. These rheological heterogeneities modulate the return flow pattern and therefore, also the geoid.

Table 1

Computed topography, tectonic stresses, geoid, admittance, and Runcorn number produced by an imposed surface velocity pattern characterized by a spherical harmonic of order $l = 4$, with a velocity parameter $v_0 = 5$ cm/yr. The 9 structures listed in column 1 all derive from the previous one and the new feature is specified.

	H m	bar	N m	Z	Ru
(*a*) Homogeneous mantle = 10^{21} p	20	302	4	0.19	0.5
(*b*) Same but with 30 times larger lower mantle viscosity	223	671	44	0.19	2.7
(*c*) Same structure with a chemical interface at 650 km	661	1 359	48	0.07	1.5
(*d*) 200 km channel with 10^{20} p rest of the upper mantle 10^{22} p lower mantle 3.10^{22} p	90	141	18	0.19	5.2
(*e*) Same structure with a chemical interface at 650 km	306	275	22	0.07	3.3
(*f*) Same structure as (d) with added 100 km weak lithosphere 10^{21} p	158	268	31	0.19	4.8
(*g*) Same structure with a chemical interface at 650 km	490	630	41	0.08	2.7
(*h*) Same structure as (f) but both layers below channel with doubled viscosity	264	362	53	0.19	6.0
(*i*) Same structure with a chemical interface at 650 km	599	739	50	0.08	2.8

CONCLUSIONS

This paper is concerned with the physical relationships between topography, lithospheric stresses and geoid undulations in a dynamical Earth. It undertook to elucidate two questions. The first is connected with the effect of sphericity, compressibility of the Earth and self-gravitation. To answer it, we investigated the response of a viscous Earth to the presence of an internal load. The latter being characterized by a spherical harmonic of order l, we showed that the above geometrical and physical ingredients play no significant role for l values larger than 10, i.e. for wavelengths smaller than 4000 km. At larger wavelengths, self-gravitation has the strongest influence. It can slightly reinforce the topography and strongly enhance the geoid by as much as 80 %, without changing tectonic stresses. For mass heterogeneities located within the lithosphere at a depth z, the induced geoid is proportional to z. This proportionality constant is weakly l-dependent, but departures from the simple moment law (2) remain moderate for realistic viscosity structures. The same is true for tectonic stresses induced by shallow sources, which are well described by the simple moment law (1). Thus, one can explain several features of the observed geoid like the linear trend away from the oceanic ridges as well as the associated tectonic stresses and topography. Small-wavelength maxima over the Altiplano in the Andes or over the Alps also stem from shallow sources. In all cases, they give rise to geoid deflections amounting to 10 to 20 m.

The second question addressed in this paper is twofold and could be phrased as follows : how deep are the sources responsible for the observed geoid at large- and moderate-wavelengths ? How can one satisfy the constraints of plate tectonics in a model Earth with a purely radial distribution of viscosity ? The analysis of a stratified Earth structure has shown the importance of expressing the spectral ratio between geoid and topography on the one hand, and between geoid and deviatoric lithospheric averaged stresses on the other hand. These two ratios are called admittance and Runcorn number. Their values for the Earth are very roughly known for small l values. It is believed that for some cases, these quantities can be negative. Here, two possible origins for the large-scale gravity perturbations are examined.

For the long-wavelength geoid undulations of amplitude approaching 100 m, it turns out that no sources located within the upper mantle can be fully satisfactory as they lead to admittances and Runcorn numbers of too small magnitude. In other words, the induced topography and stresses are much too large. More satisfactory results are derived from sources below the 650 km discontinuity if it is marked by a viscosity increase by 1 order of magnitude or more. This is especially true when no material can flow through this discontinuity. In particular, only such sources are found to yield negative values for the two ratios for low l-values. Somewhat different results might be obtained for highest viscosity in the lower mantle or in case where no lithosphere is included (Hager, 1983*b*; Lago and Rabinowicz, 1983). Within the framework of radial viscosity distributions, and for widely accepted structures like (*d*) and (*e*), it turns out that one has great difficulties in finding a mass distribution which could satisfy the global data at large wavelengths.

Features of intermediate wavelengths, say for $20 < l < 30$, could well be linked with upper mantle sources. Indeed their modest amplitudes would imply correspondingly reduced forces on the lithosphere. Negative admittance values found for zones of subduction could thus possibly be understood by the effect of a marked mantle viscosity increase, either

between lower and upper mantle (Rabinowicz *et al.*, 1983; Hager, 1983*b*), or between an asthenospheric channel and the rest of the mantle. A high viscosity lower mantle is not absolutely necessary for explaining geophysical observations correlated with subduction zones. This is suggested by cases (*b*); (*d*), and (*e*) in chapter III.

For practical purposes the following question deserves full attention. Can one use the moderate-wavelength geoid to make predictions about the prevailing tectonic stress field ? This type of approach has been promoted for the continents (Liu, 1978, 1980; Rong-shan Fu and Pei-hua Huang, 1983). It must be regarded with caution knowing that the geoid maxima over the Altiplano and the Alps correlate with extension in the first case, similarly to what is observed for oceanic ridges, and on the contrary with compression in the second case. Truly a satisfactory correlation is only to be expected if the Runcorn number is relatively insensitive to the depth and wavelength of the source density. This is the case for an homogeneous mantle structure. Figure 10 demonstrates that more realistic Earth models are incompatible with such an assumption. Hence, the elusive task of establishing the correct link between geoid and intraplate tectonics remains.

One major drawback of the Earth models with spherical symmetry is their intrinsic impossibility to generate appropriate surface velocities. Their lithosphere being continuous and homogeneous, the induced surface velocities are vanishingly small. The latter can account for intraplate deformation not for plate motion. To circumvent this limitation, a sublithospheric Earth model has been analytically treated with imposed surface velocities of adequate amplitudes. The consequences are rather striking. The predicted geoid amplitude is reasonable. The admittance and the Runcorn number are positive, and their magnitudes are of the right size. Thus the long-wavelength characteristics of the geoid associated with diverging zones, the ridges, correspond to a broad minimum. For the Earth such a feature is claimed to be superposed on the shorter wavelength maximum caused by the mass distribution in the cooling plate (Jacoby and Seidler, 1981). On the contrary, a broad maximum should correlate with subduction, i.e. zones of convergence. This is obviously true for the Earth. One has to realize that these simple models have shown that the viscosity and depth of the channel return flow are very sensitive parameters. They vary considerably between an oceanic and a continental plate or even on a regional basis. A realistic Earth model will imperatively have to integrate these lateral viscosity variations before the true contributions to the geoid to be ascribed to plate motion can be computed.

Our concluding remarks should emphasize the idea that both type of models investigated in this paper are necessary to account for the geoid. Plate motion requires a return flow generating a topography which can only be partly compensated and is hardly observable because of its small amplitude and long wavelength. Its non-dipolar nature leads to a marked contribution to the geoid, with admittances which must always be positive and cannot thereby explain all features of the measured data. Mass heterogeneities at various depths, on the other hand, can in principle provide the additional contributions to geoid, tectonic stresses and topography. The improved mapping of mantle heterogeneities by the seismologists will soon warrant detailed correlation studies with the geoid. These investigations will not only improve our knowledge of the mantle density structure, but also help to put more constraints on the lateral variations of the viscosity structure because of the necessity to take into consideration the terms describing the plate motion.

Acknowledgements

Remarks by B. Hager, H. C. Nataf and anonymous reviewers have helped to improve the final version of this paper. One of us (Y. Ricard) is supported by a fellowship from the Centre National d'Etudes Spatiales. Acknowledgement is also extended to I.N.A.G. (Institut National d'Astrophysique et de Géophysique) for the grant attributed in the framework of A.T.P. Sismogénèse (Grant n° 1150).

REFERENCES

Arthuyshkov E. V., 1973. The stresses in the lithosphere caused by crustal thickness inhomogeneities, *J. Geophys. Res.*, **78,** 7675-7708.

Cathles L. M., III, 1975. The viscosity of the Earth's mantle, Princeton University Press, Princeton, N. J.

Crough S. T., Jurdy D. M., 1980. Subducted lithosphere, hotspots, and the geoid, *Earth Planet. Sci. lett.*, **48,** 15-22.

Dalhen F. A., 1982. Isostatic geoid anomalies on a sphere, *J. Geophys. Res.*, **87,** 3943-3947.

Diament M., Sibuet J. C., Dubois J., 1983. Isostatic response of the large offset Atlantic equatorial fracture zones, submitted to *J. Geophys. Res.*

Fleitout L., Froidevaux C., 1982. Tectonics and topography for a lithosphere containing density heterogeneities, *Tectonics,* **1,** 21-57.

Fleitout L., Froidevaux C., 1983. The state of stress in the lithosphere, *Tectonics* in press.

Fleitout L., Yuen D. A., 1983. Secondary convection beneath a lithospheric plate with pressure and temperature dependent viscosity.

Gantmacher F. R., 1960. The theory of matrices, vol. II, translated by K. A. Hirsch, Chelsea Publishing, New York.

Haddon R. A. W., Bullen K. E., 1969. An Earth model incorporating free Earth oscillation data, *Physics Earth Planet. Int.*, **2,** 30-49.

Hager B. H., O'Connell R. J., 1978. Subduction zone dips and flow driven by the plates, *Tectonophysics,* **50,** 111-134.

Hager B. H., O'Connell R. J., 1979. Kinematic models of large-scale flow in the Earth's mantle, *J. Geophys. Res.*, **84,** 1031-1048.

Hager B. H., O'Connell R. J., 1981. A simple global model of plate dynamics and mantle convection, *J. Geophys. Res.*, **86,** 4843-4867.

Hager B. H., 1983*a*. Global isostatic geoid anomalies for plate and boundary layer models of the lithosphere, *Earth Planet. Sci. Lett.*, **63,** 97-109.

Hager B. H., 1983*b*. Subducted slabs and the geoid : Constraints on the mantle rheology and flow, *J. Geophys. Res.*, in press.

Haxby W. F., Turcotte D. L., 1978. On isostatic geoid anomaly, *J. Geophys. Res.*, **83,** 5473-5478.

Jacoby W. L., Seidler E., 1981. Plate kinematics and the gravity field, *Tectonophysics,* **74,** 155-167.

Jarvis G. T., McKenzie D., 1980. Convection in a compressible fluid with infinite Prandtl number, *J. Fluid Mech.*, **96,** 515-583.

Kaula W. M., 1975. Product-sum conversion of spherical harmonics with applications to thermal convection, *J. Geophys. Res.*, **80,** 225-231.

Kaula W. M., 1980. Material properties for mantle convection consistant with observed surface fields, *J. Geophys. Res.*, **85,** 7031-7044.

Lago B., Rabinowicz M., 1983. Admittance for a convection in a layered spherical shell, *Geophys. J. Roy. Astron. Soc.*, in press.

Landau L. D., Lifshitz E. M., 1959. Fluid mechanics, Course of theoretical physics, vol. 6, Transl. J. B. Sykes and W. H. Reid, Pergamon.

Lewis B. T. R., Dorman L. M., 1970. Experimental isostasy 2, An isostatic model for the U.S.A. derived from gravity and topographic data, *J. Geophys. Res.*, **75,** 3367-3379.

Liu H. S., 1978. Mantle convection pattern and subcrustal stress field under Asia, *Phys. Earth planet. Int.*, **16,** 247-256.

Liu H. S., 1980. Mantle convection pattern and subcrustal stress under the United States, *Mod. Geol.*, **7,** 81-93.

McGarr A., Gay N. C., 1978. State of stress in the Earth's crust, *Ann. Rev. Earth Planet. Sci.*, **6,** 405-436.

McKenzie D., Bowin C., 1976. The relationship between bathymetry and gravity in the Atlantic ocean, *J. Geophys. Res.*, **81,** 1903-1915.

McKenzie D., 1978. Active tectonics of the Alpine Himalayan belt : the Aegean sea and surrounding regions, *Geophys. J. Roy. Astron. Soc.*, **55,** 217-254.

McNutt M., 1980. Implications of regional gravity for state of stress in the Earth's crust and upper mantle, *J. Geophys. Res.*, **85,** 6377-6396.

Menard H. W., Dorman L. M., 1977. Dependence of depth anomalies upon latitude and plate motion, *J. Geophys. Res.*, **82,** 5329-5335.

Mercier J. L., 1981. Extensional-compressional tectonics associated with the Aegean Arc, comparison with the Andean Cordillera of South Peru North Bolivia, *Philos. trans. Roy. Soc. London,* A **300,** 337-355.

Ockendon J. R., Turcotte D. L., 1977. On the gravitational potential and field anomalies due to thin mass layers, *Geophys. J. Roy. Astron. Soc.*, **48,** 479-492.

Paquin C., Froidevaux C., Bloyet J., Ricard Y., Angelidis C., 1982. Tectonic stresses on the mainland of Greece : *in situ* measurements by overcoring, *Tectonophysics,* **86,** 17-26.

Parsons B., Daly S., 1983. The relationship between surface topography, gravity anomalies and the temperature structure of convection, *J. Geophys. Res.*, **88,** 1129-1144.

Parsons B., Slater J. G., 1977. An analysis of the variation of ocean floor bathymetry and heat flow with age, *J. Geophys. Res.*, **82,** 803-827.

Philip H., 1980. Tectonique récente et sismicité de la France, 26e G.G.I., mémoire, *B.R.G.M.*, **107,** 42-46.

Rabinowicz M., Lago B., Souriau M., 1983. Large scale gravity profiles across subducted plates, *Geophys. J. Roy. Astron. Soc.*, **73,** 325-349.

Richards M. A., Hager B. H., 1983. Geoid anomalies in a dynamic Earth. Submitted to *J. Geophys. Res.*

Richter F. M., McKenzie D. P., 1978. Simple plate models of mantle convection, *J. Geophys.*, **44,** 441-471.

Rong-shan Fu, Pei-hua Huang, 1983. The global stress field in the lithosphere obtained from the satellite gravitational harmonics, *Phys. Earth Planet. Int.*, **31,** 269-276.

Runcorn S. K., 1963. Satellite gravity measurements and the laminar viscous flow model of the Earth's mantle, *J. Geophys. Res.*, **69,** 4389-4394.

Sandwell D., Schubert G., 1980. Geoid height versus age for symmetric spreading ridges, *J. Geophys. Res.*, **85,** 7235-7240.

Schubert G., Yuen D. A., Froidevaux C., Fleitout L., Souriau M., 1978. Mantle circulation with partial shallow return flow : effects on stresses in oceanic plates and topography of the sea floor, *J. Geophys. Res.*, **83,** 745-758.

Souriau A., Souriau M., Global tectonics and the geoid, submitted to *Phys. Earth Planet. Int.*

Sykes L. R., Sbar M. L., 1973. Intraplate earthquakes, lithospheric stresses and the driving mechanism of plate tectonics, *Nature,* **245,** 299-302.

Takeuchi H., Hasegawa Y., 1965. Viscosity distribution within the Earth, *Geophys. J. Roy. Astron. Soc.*, **9,** 503-508.

Turcotte D. L., McAdoo D. C., 1979. Geoid anomalies and the thickness of the lithosphere, *J. Geophys. Res.*, **84,** 2381-2387.

Watts A. B., 1978. An analysis of isostasy in the world's ocean 1. Hawaiian-Emperor seamount chain, *J. Geophys. Res.*, **83,** 5989-6004.

Wu P., Peltier W. R., 1982. Viscous gravitational relaxation, *Geophys. J. Roy. Astron. Soc.*, **70,** 435-485.

Zoback M. L., Zoback M., 1980. Interpretative stress map of the conterminous United States, *J. Geophys. Res.*, **85,** 6113-6156.

Yuen D. A., Sabadini R., Boschi E. V., 1982. Viscosity of the lower mantle as inferred from rotational data, *J. Geophys. Res.*, **87,** 10.745-10.762.